UILU-ENG 88-3602

Report No. 141

ADHESION, MICROSTRUCTURE AND INTERFACE STUDIES OF EVAPORATED AND ION PLATED COPPER AND CHROMIUM COATINGS

by

Jeffrey C. Logas and J. M. Rigsbee
Department of Materials Science and Engineering

A Report of the

MATERIALS ENGINEERING - MECHANICAL BEHAVIOR

College of Engineering, University of Illinois at Urbana-Champaign

February 1988

Abstract

This investigation studies the relationships between the structure, the chemistry and the resultant adhesion strength of chromium and copper coatings. The coatings were produced via physical vapor deposition and ion plating (a plasma assisted physical vapor deposition technique) on copper and nickel substrates. Film adhesion, quantified using an epoxy bonded stub pull test, generally increases through the use of substrate sputter cleaning and through increasing the ion plating bias. Many structural and chemical microanalysis techniques, including SEM, TEM, EDX and Auger microprobe, are utilized to characterize the coating, the substrate and the coating/substrate interfacial region. Coating morphology changes from a fully dense and indistinct columnar structure with rounded tops to a less dense, distinct and faceted columnar structure. Energetic particle bombardment from the glow discharge creates a chemically mixed interface and causes a variation in the depth of an equiax grained nucleation layer in the coating.

Dedication

This thesis is dedicated to my wife, Lori, for her love, support, patience, and prayers during this research.

Acknowledgement

The author expresses his appreciation to Professor J.M. Rigsbee for his guidance and support throughout this research.

Special thanks are given to the past and present members of the ion plating group for their valuable assistance.

The U.S. Army Construction Engineering Laboratory is acknowledged for the use of its Ion Plating Facility. Special thanks is also due Mr. V.F. Hock of CERL for his efforts.

The support of the facilities of the University of Illinois is acknowledged, especially those of the Materials Research Laboratory Center for Microanalysis.

The author gratefully acknowledges the Army Research Office for its financial support through contract # DAAG 29-83-0151.

Table of Contents

I. Introduction

The purpose of this research program is to understand the ion plating process and to determine the relationships between ion plating processing parameters (such as sputtering and ion bombardment) and the structure, chemistry and properties of the substrate, coating/substrate interface and coating. Major effort was given to understand the nature of the interface as it often is reported that this region is primarially responsible for the properties of the coating/substrate composite.

Specifically, this research answers the following questions:

1. How does low energy ion bombardment of the substrate surface before film deposition (i.e. sputter cleaning) affect the structure of the interface and the adhesion strength of the coating/substrate couple?
2. What effect does increasing the ion flux and energy (through increasing the applied substrate bias) produce on the structure and chemistry of the interface, the morphology of the coating and the adhesion strength of the coating/substrate composite?
3. How does the mutual solid solubility of the coating and the substrate affect the structure and chemistry of the interface?

The answers to these questions provide a better understanding of the fundamental processes which make up ion plating, such as: the glow discharge phenomenon, sputtering and ion bombardment.

For this study copper and chromium were chosen as the coating materials and nickel and copper were chosen as the substrate materials because of their wide range of solubilities and crystal structures (FCC coating on FCC substrate: Cu on Cu or Cu on Ni: complete solid solubility; BCC coating on FCC substrate: Cr on Cu: no solid or liquid solubility). Substrate sputter cleaning and ion plating bias were the processing parameters this study examined in regard to their effect upon the nature and properties of the composite material.

The physical property studied in this research is the coating to substrate adhesion. Adhesion is correlated to sputter cleaning, applied bias and structure and chemistry of the interface. Microanalytical tools such as scanning electron microscopy, transmission electron microscopy and Auger electron spectroscopy are used to correlate microstructure and chemistry to the adhesion values.

II. Background Literature

A. Ion Plating Characteristics

The majority of materials failures are surface initiated by mechanisms of corrosion, wear and fatigue. One method of inhibiting surface initiated failures is to modify the chemical passivity, hardness or strength of a metal by adding alloying elements to the bulk thereby creating a metal alloy. This is inefficient and costly if the alloying elements are needed only at the surface to inhibit the initiation of the aforementioned failure mechanisms. An alternative is the use of a surface coating to concentrate alloying elements in the surface region where their effects are required.

Numerous coating techniques have been developed each having its own effects upon critical coating/substrate characteristics such as:

1. the adhesion between the coating and the substrate;
2. the chemistry and the microstructure of the coating;
3. the chemistry and microstructure of the coating/substrate interface;
4. the uniformity and thickness of the coating;
5. the bulk physical properties of the coating; and
6. the porosity of the coating [1].

Thus a coating technique is chosen which best produces the coating characteristics desired. A review of the advantages and

disadvantages of the many coating techniques will not be presented here, but may be found in a review article by Bunshah [2].

The potential advantages of ion plating are many as this process is reportedly capable of producing coatings which meet the previously named critical coating/substrate characteristics. Primarily, ion plating produces coatings which exhibit excellent coating adhesion due to the chemically graded interface resulting from ion-induced mixing and recoil implantation processes [3], which are discussed in a later section. Other major advantages of ion plating include: 1) its ability to deposit metals, alloys and ceramic materials onto almost any substrate material (the use of nonconducting substrates requires minor technique modifications [4]) regardless of its thermal expansion coefficient; 2) the high "throwing power" (or the ability to uniformly coat all exposed substrate surfaces) resulting from gas scattering and redeposition of atoms sputtered from the surface allows complex parts to be uniformly coated with little or no specimen movement [5] and 3) production of a dense microstructure with equiaxed grains without applied substrate heating [6].

The two major disadvantages of ion plating both arise from it being an in-vacuum process. First, ion plating requires sophisticated electronics and vacuum equipment similar to that of sputter deposition. Second, it is slower than "in-air" techniques such as flame spraying or plasma spraying.

B. Ion Plating Background

Ion plating is a hybrid process combining facets of vacuum evaporation and sputtering while also encorporating the benefits of "sputter cleaning" and ion beam mixing. Ion plating usually occurs in an inert gas (around 10^{-2} Torr) glow discharge similar to that of sputter deposition, except the substrate holder is the high voltage (2-5kv) sputtering cathode. An essential feature of ion plating is substrate surface "sputter cleaning" prior to coating deposition. Sputter cleaning occurs as the substrate holder (cathode) is subjected to inert gas and neutral atom bombardment. After sputter cleaning, evaporation begins along with continued ion and neutral atom bombardment of the cathode. Thus for net film growth to occur, the deposition rate must exceed the sputtering rate.

Sputter cleaning often is proposed as a critical factor in causing the excellent adhesion of ion plated coatings as compared to the adhesion of other vacuum evaporation processed coatings. Inert gas ions from the glow discharge are accelerated toward the cathode and strike the substrate surface with sufficient kinetic energy to remove (sputter) atoms from the surface [7]. The sputter cleaned surface is atomically clean [8] and therefore very reactive [9]. This clean and active surface is ideal for coating as it contains many likely sites for nucleation [10,11] and the high energy ion/atom flux increases the adatom mobility which in turn increases surface diffusion and surface mixing as

well as growth of nuclei. After thorough sputter cleaning evaporation of the coating material is begun while glow discharge sputtering continues. Conventional resistance heating may be used to evaporate low melting point materials while high melting point materials are usually evaporated using electron beam heating.

As the coating atoms begin to reach the substrate many processes happen simultaneously: energetic ions and atoms can be implanted into the substrate; substrate atoms can be sputtered and some of these can be recoil implanted into the growing film; deposited coating atoms can be sputtered off of the surface and then redeposited and gas atoms may become entrapped by the growing film. Mattox supplies a schematic representation of the possible events [12].

Only a small percentage (less than 1%) of the evaporated atoms are ionized through collisions with metastable inert gas ions [13] and are accelerated toward the substrate by the high negative potential of the substrate holder. Very few ions arrive at the cathode with the full energy of the discharge because the gas pressure is high (about 10^{-2} Torr) and therefore, the mean free path is short (5 mm) compared to the cathode dark space to substrate holder distance. Thus each accelerating ion will likely undergo multiple collisions with evaporant atoms or inert gas atoms. Each collision causes a kinetic energy and direction transfer. Experimental measurements by Teer [14] have shown the energy of ion and evaporant atoms deposited at the substrate to be less than 100eV. Typically 90% of the deposited energy is

carried by atoms (both inert gas atoms and evaporant atoms) not ions.

Thc coating deposition rate is the difference between the rate at which atoms arrive at the surface and the rate at which atoms are sputtered away from the surface. The deposition rate, therefore, can be cotrolled mainly by the evaporation rate but also by the energy of the glow discharge.

The multiple collisions and momentum transfer between ions and atoms benefit the ion plated coating three ways. First, atoms and ions impinging on the substrate have high average kinetic energy. Thus atoms are implanted up to several atom layers deep into the substrate surface [15,16]. This causes extensive localized mixing due to kinetic energy transfer from the impacting particle to nearby substrate atoms. This ion-enhanced mixing between the depositing atoms and the substrate atoms creates a strong metallurgical bond at the coating/substrate interface and is responsible for the excellent coating adhesion of ion plated coatings. The graded coating/substrate interface is characterized by a gradual transition from the substrate chemistry and microstructure to the coating chemistry and microstructure. This gradient minimizes stress concentration at the interface due to externally applied forces or stress arrising from differences in thermal expansion coefficients. Although a graded coating/substrate interface usually can be created by a post deposition heat treatment [17], ion plating requires minimal substrate heating (hence little alteration of temperature dependent substrate mechanical

properties) and allows materials with limited mutual solid solubilities and low diffusivities to mix (the reported depths are up to 25 μm for ion plated Au on Al [17] or 5 μm for Cu ion plated onto steel [18] which may be overestimted due to the methods of analyses).

The second advantage of the momentum transfer process in ion plating is the effect of the energized particles on the coating microstructure. Raising the average kinetic energy of the depositing atoms has the same effect on the coating microstructure as raising the substrate temperature [19,20]. Using low kinetic energy (below 0.2 eV) evaporated atoms requires the substrate to be heated to half the melting point of the coating if a fully dense, equiaxed grain coating is to be produced [21]. Ion plating can produce a similar coating with little or no substrate heating [19,20,22]. As previously mentioned the sputter cleaned surface is atomically clean with a high concentration of defects which serve as active coating nucleation sites [23,24]; depositing atoms have high surface mobility (due to high average kinetic energies) which allows them to migrate to form stable nuclei. This increases the nucleation rate/growth rate ratio.

The third benefit of particle bombardment involves the throwing power of the ion plating process. Throwing power is the ability to produce nearly uniform coating thicknesses over the entire surface of even complexly shaped substrates [25]. The extensive scattering which occurs durring ion plating and the tendency of scattered ions to follow the electric field lines

produce a nearly constant rate of deposition on all exposed regions of the substrate.

C. Ion Plating Applications

Ion plating was developed by Mattox [26] in 1964 as a method of depositing Al coatings to prevent oxidation of uranium fuel elements. Commercial ion plating applications have been successful in protecting surfaces in corrosive or wear environments. Yet the number of commercial applications of the ion plating technique is small when compared with other surface coating techniques.

The first commercial application of ion plating was the production of corrosion and oxidation resitant aluminum coatings on uranium fuel elements [26,27]. In this case the uniform thickness and excellent adhesion of the aluminum coating prevented spalling in spite of the temperature cycling. Ion plated aluminum coatings are also used for inhibiting stress corrosion of titanium and steel fasteners for aircraft and spacecraft [28,29].

Ion plated coatings have been used successfully as tribological coatings. The technique was developed by Bergbars [30] and is noted for good adhesion and dense structure. Coatings of Au, Ag, MoS_2, Cu-In and Cu-Pb have been produced and operate successfully as dry lubrication in vacuum environments, at very low temperatures or in nuclear power plants where conventional lubricants such as oil and grease fail [30-32]. The

superior adhesion of the ion plated hard coatings, in addition to the reduced friction coefficients, are responsible for the increased lifetimes compared to coatings produced by other techniques. Wear resistant TiN and TiC coatings on tool steels [32-37] produced by reactive ion plating (where a portion of inert gas in the chamber is replaced by a reactive gas such as nitrogen and an enhancement (second anode) system is used during ion plating to more completly ionize the gas/evaporated metal atoms for increased chemical reactivity) yield increases in tool life of up to 10 times.

D. Components Of Ion Plating

Ion plating is a complex process which is more easily understood when it is divided into a series of processes (glow discharge, sputtering, evaporation and ion bombardment). Therefore, a brief presentation of these processes will be presented here.

1. Glow Discharge

Ion plating is a glow discharge assisted physical vapor deposition technique. Ion plating often is erroneously labeled a plasma aided physical vapor deposition technique. A plasma, however, is characterized by being nearly homogeneous with a well-defined potential and density with constituent particles in equilibrium motion [38]. Glow discharges only approximate the

conditions of a plasma.

A glow discharge can be produced by applying a potential across two electrodes in a gas. This requires that ion plating occur in a soft vacuum (5-10 milliTorr). If the pressure is too low no discharge can be established. A d.c. glow discharge can be divided into three regions: 1) the cathode region; 2) the glow region and 3) the anode region. The cathode region (of great interest as it is the region nearest the substrate) is the area between the cathode and the glow region. The cathode is biased negatively (typically 2-5 kv) above the breakdown voltage or else an auxilliary source of electrons is needed to compensate for those which leave the glow region by electron-ion recombination at the anode (generally at the chamber walls) and in the gas. The negative bias of the cathode attracts positive ions and supplies secondary electrons needed to sustain the glow. The cathode region is also characterized by an accumulation of positive ions near the cathode. Electrons from the cathode are accelerated across the cathode region (also known as the dark space or the cathode fall space) by the positive space charge toward the glow region (an electrically neutral region). The extent of the dark space is about equal to the distance traveled by an electron between ionizing collisions. This may be five to ten times longer than the mean free path which includes other types of collisions. The electric field across the dark space varies linearly from the cathode to the glow region [39] and the maximum kinetic energy of the electrons is obtained at the edge of the glow region.

The cathode region also contains a thin glow region adjacent to the cathode. This glow occurs when an electron of most probable energy causes an excitation event for a support gas atom. For argon this excitation event is most probable for electrons of 100 eV [39].

Electrons of high kinetic energy from the cathode collide in the glow region with support gas atoms producing electron-ion pairs ($e^- + Ar \rightarrow Ar^+ + 2e^-$). The electrons produced in the collision can be accelerated and produce more electron-ion pairs. The glow is produced when a support gas atom undergoes a deexcitation event and produces a photon with a wavelength in the visible spectrum. The extent of the glow is determined by the energy of the electrons from the cathode. The location where the electrons have lost enough energy that they no longer can produce electron-ion pairs defines the edge of the glow. Here low energy electrons accumulate without producing ions causing a dark region called the Faraday dark space.

Since the glow region is electrically neutral, the positive ions move slowly (through diffusion) until they reach the edge of the cathode dark space. The ions are accelerated toward the cahode (substrate holder); this is the primary benefit of the glow discharge. Before reaching the cathode an ion is likely to undergo numerous momentum transfers and charge exchange events with support gas atoms or evaporant atoms in the cathode region. The energy distribution of ions reaching the cathode is dependent upon the mean free path of ion-atom collisions. Theoretical calculations by Davis and Vanderslice [40] show that most of the

ions reach the cathode with negligible energy. Most of the cathode bombardment is due energetic neutrals. Expermental work by Houston and Uhl [41] and Armour et al. [42] has confirmed this theory.

The anode region exists from the glow region to the chamber walls (anode). However, in most glow discharges used for deposition the electrodes are so close to each other that the anode region is absent except for the anode itself. This does not extinguish the glow discharge as it is only dependent upon electron emission from the cathode. It will suffice to say that in the anode region electrons exit the glow discharge at the anode. These electrons must be replaced at the cathode or the glow will be extinguished. For more information about glow discharges the reader is referred to the text by Chapman [43].

2. Ion Bombardment

The bombardment of the substrate and coating with energetic particles is the purpose of the glow discharge. Mattox [44] has divided the effects of ion bombardment into three areas: before deposition, at the onset of deposition and during film growth. The purpose of the glow discharge prior to deposition is to clean the substrate by sputter removal of contaminants through particle ejection following a multiple collision process between the energetic particle and the substrate surface. This process is known as sputter cleaning. The removal of surface contaminants provides a nearly atomically clean surface on which the film is

deposited. The bombardment may also produce surface defects and alter the surface morphology and crystallography. Sputter cleaning is a key feature of ion plating. The events occuring during sputter cleaning are more throughly discussed in a later section entitled "Sputtering."

The formation of the interface between the substrate and the coating at the onset of deposition plays a major role in the final properties of the coating/substrate composite. The effects of ion bombardment are many during interface formation. The effects include: a local increase in temperature (due to energy dissipation from the incident energetic particles) which promotes diffusion and the resultant high defect concentration which also aids diffusion. As mentioned earlier ion bombardment also causes physical mixing of the film and substrate particles through implantation, sputtering and redeposition and lastly recoil deposition. All of these processes promote the formation of a diffusional or pseudu-diffusional graded interface.

Particle bombardment will likely determine the mode of nucleation of the film. If the bond strength between the condensing atom and the substrate is weak then the surface mobility of the atom will be large. The atom will condense only at high energy sites: defects or by colliding with other coating atoms. Particle bombardment produces many defects and thus enhances island formation. A strong bond, however, requires the mobility to be low thus producing a continuous monolayer.

The most studied and most published effect of ion bombardment is during coating growth [45-47]. It effects crystallography,

morphology and resultant physical properties. It also may enhance or diminish prefferential growth by altering the surface temperature.

Movchan and Demichishin [45] were the first to develop an empirical relationship between evaporated thin film microstructure and processing parameters (substrate temperature). Three characteristic zones were established relating the substrate temperature (normalized to the melting point of the coating) to the grain structure obtained from simple evaporation (figure 1). Zone 1 (at temperatures below T1) contains separated columnar grains with domed tops. Zone 2 (between T1 and T2) is characterized by densely packed columns with well defined boundaries and a smooth surface. Zone 3 (above T2) has well defined, densely packed, equiaxed grains.

Thornton [46] added a pressure dimension to this diagram (figure 2). This still does not account for the effects of ion bombardment. The Thornton diagram inserts a transition zone (Zone T) between Zone 1 and Zone 2. The structure of Zone T is that of densely packed, poorly defined, fibrous grains.

The extension of this diagram to ion plating is common. The general effect of ion bombardment is to shift the morphology to that of increased temperatures. Thornton [47] attributes the suppression of the columnar morphology to redistribution of coating material due to sputtering.

Other properties effected by ion bombardment include adhesion (discussed in a later section entitled "Adhesion") and intrinsic stress. Evaporated coatings have a tensile stress while sputter

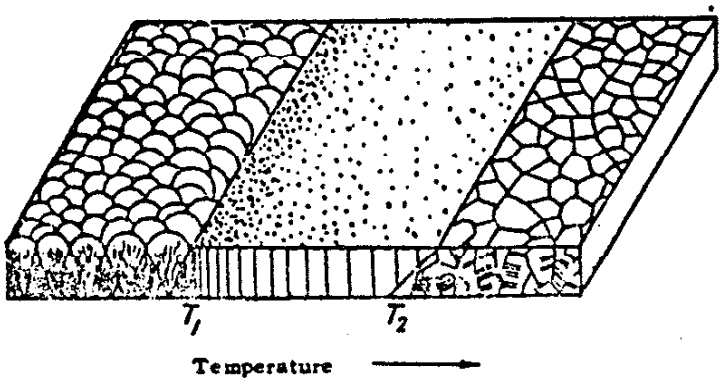

Figure 1 - Movchan - Demchisin zone structures [45]

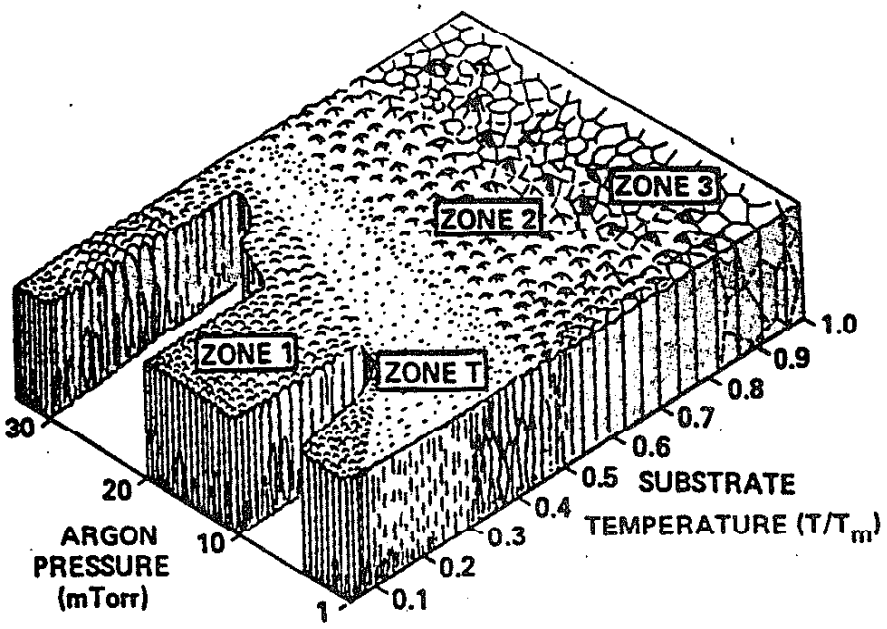

Figure 2 - Thornton zone structures [46]

deposited coatings contain a compressive stress.

3. Sputtering

Ion plating systems do not require the use of a sputter source to deposit a film, however, sputtering of the substrate and the growing coating occur as a result of particle bombardment supplied by the glow discharge. In ion plating sputtering occurs before deposition (sputter cleaning), during coating nucleation and coating growth. Sputtering may be defined as the removal of a surface atom by the transfer of momentum and energy from incident particles. A thorough review of sputtering is found in reference [48].

The fundamental process is the atomic collision modelled as a binary, hard sphere, elastic collision. Due to geometric considerations, a single collision can not cause ejection of a substrate atom. Thus sputtering theories rely upon multiple collisions. Since momentum is most efficiently transfered by collisions of particles with similar masses, the inert support gas in the glow discharge usually chosen is argon.

Sputter efficiency mainly is determined by the sputter yield parameter, S, that is the number of target atoms ejected per incident particle. Generally, S depends upon several variables: 1) the mass of the target atom; 2) the mass of the incident ion or atom; 3) the atomic number of the target material; 4) the energy of the incident particles and 5) the angle of incidence of the particles to the substrate. Sputtering has been divided into

three categories according to energy. These are:

1. low energy or light ion sputtering (below 10^3 eV)
2. linear cascade sputtering (10^3-10^5 eV)
3. non linear cascade sputtering (above 10^5 eV)

Low energy sputtering is characterized by sputtered atoms lacking sufficient energy to produce recoil cascades. Linear cascade sputtering is noted for recoil cascades where only a small fraction of the atoms in the cascade volume are in motion. The high energy non linear cascade regime is characterized by most of the atoms in the cascade volume moving due to collisions with recoil atoms. In ion plating only low energy and linear cascade sputtering are imporant. Although each sputtering regime has been modelled (emperically or theoretically) the best understood is linear cascade sputtering. In the model developed by Sigmund [49] the expression for the sputtering yield, S, due to an orthogonal beam is

$$S(E,\Theta=0) = 0.042^{-2}\alpha(m_t/m_i)S_n(E)U_o^{-1} \qquad (1)$$

where U_o is the binding energy of the surface target atoms, $S_n(E)$ is the molecular stopping cross-section and $\alpha(m_t/m_i)$ describes the momentum transfer between the incident ion and the target atom. The maximum sputter yield occurs at angles less than orthogonal [50] as ions of less than orthogonal incidence require fewer collisions to sputter a target atom. The sputter yield for most metals ranges from 0.5 to 5.0 and is not temperature dependent. For glow discharge sputtering (low energy

sputtering), as in ion plating, isotropic cascades no longer occur and theories such as Sigmund's no longer are valid. Bohdansky et al. [51] had success emperically modelling sputtering in this regime. The sputtering rate relative to the deposition rate may significantly effect coating morphology [44]. Preferential sputtering and induced surface topography also result from sputtering when a multicomonpent or a non planar target is utilized [43]. Removal of the element with the greater sputter yield will occur preferentially until the average surface concentration has equilibrated. Hence,

$$S_a\Theta_a/C_a = S_b\Theta_b/C_b \qquad (2)$$

where S_a and S_b are the sputter yields of materials A and B respectively, Θ_a and Θ_b are the surface concentrations of A and B and C_a and C_b are the bulk concentrations of A and B [52]. The topography is the result of the variation in the angle of incidence of the particle to the non planar surface causing changes in sputter yields. For ion plating surface topography due to sputter cleaning may act as preferential nucleation sites.

4. Vacuum Evaporation

In all vapor deposition techniques the coating material must be vaporized for film formation. Electron beam evaporators are the most common method of producing the vapor for the ion plating process. Evaporation occurs when particles of a condensed phase are ejected due to induced thermal heating. In vacuum

evaporation, evaporation of the coating material occurs when the vapor pressure exceeds the pressure in the vacuum chamber. From classical thermodynamics, phases in equilibrium must have equal values of chemical potential, μ. For evaporation the chemical potential of the vapor must equal the chemical potential of the liquid ($\mu_l = \mu_v$) and for sublimation the chemical potential of the solid must equal the chemical potential of the vapor ($\mu_s = \mu_v$). The Clausius-Clapeyron equation [53] is derived from these relationships. This equation

$$\frac{dp^*}{dT} = \frac{H_g - H_c}{T(V_g - V_c)} \qquad (3)$$

defines the equilibrium pressure change due to an incremental temperature change resulting from the difference in the enthalpies of gas and condensed phase and the difference in the volume of each phase. By combining classical thermodynamics and the kinetic theory of gases reasonably accurate quantitative expressions for evaporation rates can be derived. Hertz and Knudsen [54] developed a relationship for the number of atoms evaporating from a surface of area A_e during an incremental time dt

$$\frac{dN_e}{A_e dt} = \alpha(2\pi mkT)^{\cdot 5}(p^*-p) \text{ cm}^{-2} \text{ s}^{-1} \qquad (4)$$

where p^* is the equilibrium pressure and p is the return flux, m is the molecular weight, k is Boltzmann's constant and T is temperature in degrees Kelvin. The Hertz-Knudsen equation gave

rates always greater than expermentally achieved. Thus the coefficient, α, which came to be known as the evaporation coefficient was introduced to match experimentally observed rates. The evaporation coefficient ranges from zero to unity and is highly dependent upon the cleanliness of the source surface. Atoms are emitted from the source with an average energy of 1.5 kT. Atoms also follow a cosine law for spatial distribution [54]. This cosine law breaks down in ion plating conditions due to the high pressure and resulting large amount of gas scattering.

Evaporation is performed by two principal methods: resistive heating and electron beam heating. In ion plating electron beam heating is the more common method. Current electron beam guns have self-contained anodes and magnetic deflection systems. The filament is maintained in a chamber differentially pumped from the chamber in which the glow discharge occurs. The filament is thus opperated at a lower pressure (10^{-5}Torr) to extend its lifetime. The beam passes through a small hole separating the chambers and is bent 270 degrees to reach the evaporant material. The advantages of the electron beam sources include their ability to evaporate refractory metals and ceramics. A general discussion of evaporation sources can be found in reference [54].

E. Adhesion

Adhesion, the bonding of the coating to the substrate, is a major factor in determining the effectiveness of a

coating/substrate couple. The term has many meanings but is most often used to qualitatively or quantitatively describe the strength of the coating/substrate bond and thereby determine the in-service usefullness of the coating/substrate system. However, adhesion is also used to describe the fundamental atomic bonding between the coating and the substrate.

Mital [55] has done an excellent job reviewing adhesion terminology and the factors affecting adhesion. He subdivides adhesion into "basic adhesion" and "practical adhesion." The term "basic adhesion" describes the interfacial bond strength (i.e. summation of interatomic forces such as electrostatic, chemical or Van der Waals) which is solely dependent upon interfacial properties. Basic adhesion measurement techniques are reviewed by Campbell [54] and include nucleation rate measurements, island density measurements, critical condensation, residence time and microcalorimetry measurements. Extreme caution is necessary to ensure only interatomic forces are measured and not those of the bulk coating/substrate composite.

Properties of the bulk coating/substrate combination are included in "practical adhesion" data and may include intrinsic stress, film thickness, sites of easy failure and the method of applying the external stress. Because of the many bulk properties affecting practical adhesion, there may be no simple relationship between practical adhesion and basic adhesion. Mital [55] describes practical adhesion as the force or work required to detach or separate adhering phases. This separation can occur at the interface, in the interfacial region or in the bulk of the

weaker region. Good [56] suggests the use of microchemical methods such as electron spectroscopy for chemical analysis (ESCA) or Auger electron spectroscopy (AES) to determine whether the separation occurs at the interface or at an interfacial region. Failure often occurs at a weak boundry layer such as a brittle oxide of a metal.

Techniques of measuring practical adhesion include topple, tape, peel, scratch and tensile tests. Many of these are explaind by Campbell [54]. Since practical adhesion is generally measured and reported, adhesion will henceforth be understood as pratical adhesion unless otherwise specified.

Mital [55] notes the importance of adhesion measurements for defining optimum coating process variables and substrate prepartions. The data may be used simply to discriminate parts with poor adhesion strength from those with acceptable strength. However, in order to understand the adhesion data Campbell [54] suggests one must correlate the the data with both process parameters and the structure of the coating and the coating/substrate interface.

The importance of the properties of the interface is apparent to Mattox [57] who reports good adhesion is promoted by 1) strong atom-atom bonding within the interfacial region; 2)low local stress levels; 3) absence of easy deformation or failure modes and 4) no long term degradation modes. As these characteristics are dependent upon the nature of the interface, likewise, the interaction between the depositing atoms and the substrate determines the interfacial nature. Atoms impinging on a surface

eventually lose their kinetic energy and condense to form stable nuclei [54]. The amount of the kinetic energy and the strength of the interaction between the adatom and the surface determines the surface mobility of the adatom. A strong atom-surface interaction produces a high nuclei density, while a weak interaction gives widely spaced nuclei. These nuclei grow to form a continuous film. The growth mode and nuclei density determine void development and thereby the effctive interfacial contact area and ultimately the adhesion strength [58]. The nuclei density is dependent upon ion bombardment, electric fields, gaseous enviornment, contaminant layers, surface impurities, surface defects and deposition technique.

Mattox [59] lists five types of interfacial regions which are formed due to different interactions between the adatom and the surface. A mechanical film relies upon mechanical interlocking of the film with a rough surface to provide its strength. A monolayer to monolayer interface is characterized by an abrupt change from the film to the substrate. As there is no chemical reaction or diffusion allowed in this type of interface, often due to low solubilities, the interface is only 2-5 A wide or about the atomic spacing. A constant composition layer, many lattice parameters wide, characterizes the compound interface. It is created by a chemical reaction between the film and substrate. The compound may be an intermetallic or an oxide, for example, and is usually brittle. Other problems with the compound interface include: physical and chemical discontinuities due to abrupt phase boundaries [60], impurity segregation at

phase boundaries, porosity and stresses due to lattice mismatch. Diffusion type interfaces exhibit a gradual change in composition, intrinsic stress and lattice parameter across the interfacial region and require elevated substrate temperatures during coating. The use of high energy adatoms by such techniques as ion plating or ion bombardment can produce a "pseudo-diffusion" type of interface even at low substrate temperatures or for materials which are mutually insoluble [3]. Ion bombardment prior to film deposition may produce high concentrations of point defects or stress gradients which promote diffusion. Combinations of these interface types are possible.

Generally the adhesion between nonsoluble, non-compound forming coating substrate pairs is weak unless an energetic coating process is used. Alternatively, an intermediate layer which reacts with both the coating and the substrate may be used to improve adhesion by forming compound or diffusional interfaces.

As stated earlier there are numerous methods of measuring adhesive strength reported in the literature. The adhesion tests are generally of two types: tensile and scratch. The tests range from the simple and qualitative (Scotch tape test) to the complex and quantitative (scratch test or direct pull tensile test).

Swaroop and Adler [61] used a 90 degree bend test and Scotch tape test to check the adhesion of both ion plated and thermally evaporated copper films on steel substrates. The bend test involved putting the sample in a vise and bending it 90 degrees

in a continuous motion. The sample was then examined with an optical microscope to look for cracks. Cracks were found in the evaporated coating only. The Scotch tape test used Scotch Brand no. 810 tape, which has an average pull strength of 2000 g/cm^2. Again only the evaporated coating failed.

Jacobsen and Kruse [62] used the more quantitative direct pull method to test the adhesion of evaporated silver on unheated BK7 glass substrates. Cold setting Cyanolite 202 cement was used to bond cylindrical steel blocks to the coating. After the cement hardened the blocks were pulled perpendicularly from the coating. The stress (σ) required to remove the coating is defined by

$$\sigma = F/A \qquad (5)$$

where F is is the applied force and A is the area of the steel block. The average adhesive strength was 231 kPa/cm^2.

Jacobsen and Kruse [62] also analyzed the influence of errors in allignment of experimental set-up and non-uniformities of the cement used to remove the coatings. Misalignment by 0.001 radians causes a moment of 10 kPa mm and shear stresses ranging from 7 to 20 kPa/cm^2 in addition to the normal stress. The non-uniformity of the cement thickness causes the reported force to be 5% too low. These errors account for only 25% of the range of adhesion values they report.

The direct pull technique was also used by Varchenya and Upit [63] to measure the adhesion of copper, silver, gold, indium, tin

and lead on quartz cleaved in vacuum and in air prior to deposition. The adhesive strength was assessed by attaching a 3 mm pin to the coating using epoxy resin cured for 3 hours at 40°C. The height of the pin was equal to its diameter in order to reduce stresses due to misalignment. The adhesive strength was always small (about 10 MN/m^2) with the freshly cleaved samples having only slightly better adhesion than the cleaved in-air samples. The metals chosen do not react chemically with quartz at room temperature. Aluminum does react with quartz at room temperature and forms Al_2O_3 and silicon. Because of this reaction the adhesive strength measured was 50 MN/m^2.

A trend of adhesive strengths was noted for the subgroups IB(Cu,Ag,Au), IIIB(Al,In) and IVB(Sn,Pb). The adhesive strength decreases within a given subgroup as the atomic number increases. The free electrons for group IB are s electrons while for groups IIIB and IVB the free electrons are sp electrons. Thus the result is that the strongest bonding occurs between quartz and a metal which has the highest density of free electrons within the group of elements under consideration (e.g. Cu in group IB).

A commercially available direct pull adhesion tester called the Sebastian I Coating Adherence Tester (manufactured by Quad Group Inc., Santa Barbara, California) was used by Salem and Sequida [64] and Mirtich [65] to measure adhesion strength. Aluminum pull stubs, precoated with epoxy, are attached to the substrate and cured at 150°C for an hour. The stubs are pulled normally to the coating until failure occurs. The epoxy failure strength is rated at 45-62 MPa (65-90 ksi) while the instrument

has a maximum load rating of 71 MPa (10.3 ksi). The major drawback of this technique is the the epoxy (rated at least 9 MPa less than the instrument's maximum load capability) which often fails before the coating is removed from the substrate. The applied stress is not actually the true failure stress because there exists an unresolved triaxial stress at the intersection of the epoxy adhesive at the film surface. A third problem will arise if the epoxy fails to flow sufficiently to make contact over the entire surface of the stub. This reduces the loaded area and causes a lower adhesion strength to be recorded. The advantages of the Sebastian test unit are its quantitative nature and its wide use due to being commercially available.

Salem and Sequida [64] noted an increase in adhesion strength of gold coatings on alumina substrates which received argon or oxygen ion beam surface modification prior to deposition. Mirtich [65] also noted good adhesion (exceeding the failure strength of the epoxy) for many ion beam sputter deposited metals on H13 steel only if the steel substrates were cleaned by the ion beam before deposition. The strength of the films was independent of film thickness between 1 μm and 8 μm.

Stoddart et al. [66] studied the adhesion of copper films vapor deposited onto soda lime glass and silica substrates. The effect of glow discharge surface treatment on adhesion was reported using a tensile test. Brass rods were glued perpindicularly to the film using a quick setting cyanocrylate adhesive (Eastman 910). A tensometer and load cell were used to apply and measure a horizontal force. Organic contamination was

removed by the glow discharge which improves adhesion. Auger studies revealed that gases are also desorbed from the substrate surface. Stoddart, upon examining broadface TEM samples, also noted a further effect of the glow discharge on adhesion of copper films vapor deposited on glass and silica substrates is the increased density of coating nuclei and enhanced lateral growth. The nuclei may act as sites of stronger binding or "pinning" sites thus enhancing adhesion. There was no evidence of vacuum chamber materials being sputtered onto the substrate nor was there evidence of micro-roughening of the surface.

Kikuchi [67] used a "topple" test to measure the adhesion of silver films on discharge cleaned glass substrates. The topple test involves securing a stainless steel cylindrical rod of radius 6 mm and height 50 mm to the coating using an epoxy cement cured at room temperature for 24 hours. The top of the rod was connected by a horizontal spring to a motor. Linearly increasing forces were applied to the top of the rod until the film peeled off. The peeling force, F, was recorded and is related to the adhesion strength, σ, by the equation

$$\frac{\sigma}{} = \frac{4hF}{\pi r^3} \qquad (6)$$

where h and r are the height and radius of the rod respectively. The topple test was accompanied by a scratch test using pencil lead of various hardnesses (determined by a Vickers microhardness tester) as the styli. The leads had a radius of curvature of 0.25 mm. A load of 120 g was applied to each stylus and the scratch length was 10 mm. Peeling was generally present with the

peeled length determined using a microscope. The reported adhesion is about 10 MN/m^2 and is independent both of thickness between 820 A and 2120 A and deposition temperature below 200°C. Ion bombardment of the substrate produced a time dependent improvement of adhesion which appeared gradually after deposition. The adhesion of films measured 75 days after deposition improved by a factor of 2.5 over the initial values. Lastly, the adhesion of the topple test and the scratch test length are related in a monotonic fashion.

A scratch test of a different type is reported by Perry [68] for determining the adhesion of TiO_2 on glass substrates produced using evaporation, plasma discharge sputtering and ion plating. This scratch test involves pulling a Rockwell "C" diamond indenter with a hemispherical tip of 200 μm radius across the coating. Successive scratches using increasing force were produced until the coating was removed. The reported adhesion value is the load required to remove the coating . Determining the failure load is not easy as failure may occur within the film.

When selecting an adhesion test consideration should be given to the type of information which is required. If one is interested in "basic adhesion," a complicated nucleation rate, island density, critical condensation, residence time or microcalorimetry measurement must be performed. The choices to measure "practical adhesion" are simpler, but care must be taken to consider the properties of the coating/substrate couple. The Scotch tape test is the simplest but offers little information.

Scratch tests, however, are usefull for coatings with high adhesion strength, but ductile films present a problem. The Sebastian adherence tester and other direct pull methods are easy to perform, work well on ductile films but give little information when the adhesion strength exceeds that of the epoxy. The limitations of an adhesion test along with the properties of the coating/substrate couple must be carefully examined in order to choose an affective adhesion test.

F. Review of Related Experiments

As a conclusion to the background section of this thesis four studies of ion plated and evaporated copper and chromium coatings are reviewed. Abermann and Martinz [69] vapor deposited chromium coatings onto glass substrates at five different substrate temperatures ranging from 25°C to 460°C. The grain size of the coatings, as viewed in broadface transmission electron micrographs, increases by a factor of ten at higher substrate temperatures. The increase is most pronounced above 300°C.

Chromium coatings were also deposited on glass substrates maintained at 460°C for various thicknesses. At 150 Å the coatings are made of discontinuous islands. At 290 Å the coatings are mainly continuous, but a limited number of holes and channels still exist. At 700 Å the coatings are clearly continuous and dense and have a grain size 20 times as large as the 150 Å thick coating.

Copper coatings were ion plated onto steel substrates using

the conventional diode method of ion plating (180°C substrate temperature) and by using a thermionically assisted triode (electron enhanced glow discharge) method (290°C substrate temperature) by Kloos et al. [31]. They report good adhesion for the coatings with no detectable difference between the coatings. Vacuum evaporated copper coatings, however, spalled with no applied force due to high internal stress. The structure of the diode coating is a zone 1 type with domed tops, large grain size and a rough surface. The triode assisted coating is refined; the grain size is smaller and the coatings are denser. This most likely is due to the enhanced glow discharge, but may also be influenced by the higher deposition temperature.

Teer and Delcea [19] studied the structure of ion plated copper coatings on nickel substrates using scanning electron microscopy. Bias voltage was varied from 2 kV to 5 kV; argon pressure was varied from 20 mTorr to 40 mTorr and bias power density was varied from 0.77 W/cm^2 to 2.5 W/cm^2 at nearly constant substrate temperatures (about 200°C). They report five important results:

1. Coating structures similar to the zone 1 structures of Movchan and Demchisin are produced by ion plating at low bias power densities.
2. At higher power densities denser structures (zone 2) are produced. A further increase in bias power density produces dense structures with a grain size of about 1 μm.
3. Use of a triode enhanced glow discharge increases the bias power density and results in dense coatings with a very

fine grain size (about 0.1 μm).

4. The significant cause of the densification of the coating structure is the high surface temperature.
5. Dense coatings can be produced by ion plating at low substrate temperatures.

Walls et al. [70] studied the coatings discussed above (referance 19) using optical microscopy and Auger electron spectroscopy. The interfaces, which were clearly visible for polished and etched samples under the opticl microscope, exhibited a depth of 25 μm. The Auger electron analysis confirmed this depth and used a probe 3 μm in diameter. They report no difference in interface depth for copper coatings produced on nickel substrates using vacuum evaporation and ion plating. They suggest this result is due to copper and nickel being mutually soluble in the solid phase.

III. Experimental Equipment and Procedure

A. Ion Plating Facility

The coatings in this study were produced using the Ion Plating Facility which is located at the Construction Engineering Research Laboratory (CERL) operated by the U.S. Army Corps of Engineers in Champaign, Illinois. The ion plating system was manufactured by Torr Vacuum, Inc., located in Van Nuys, California.

The system utilizes a split chamber design which allows for easy access to the interior. The vacuum chamber is made of 304 stainless steel. The upper chamber is raised by a mechanical hoist and may be pivoted about the hoist axis as needed. All chamber vacuum seals are the rubber "O ring" type except for conventional conflat feedthroughs. The entire chamber is water cooled to prevent damage to the rubber "O rings." The chamber is cylindrical with a diameter of 0.66 m. Both the upper and the lower chambers contain a variety of access ports in order to accomodate a variety system accessories. The upper chamber also has two 0.115 m diameter viewports that allow observation of the inside of the chamber during coating deposition. Disposable glass inserts protect the windows of the viewports from coating, thus minimizing down time. A "baffle plate" is placed in the

lower chamber. This allows differential pumping and isolates the electron gun filament from the higher pressure, which is needed to support the glow discharge, of the upper chamber. The substrate holder also is made of 304 stainless steel. Its distance from the source is adjustable; in this study the source to substrate distance was kept constant at 0.254 m. The substrate holder is water cooled and is welded to a pipe which passes through the chamber lid. Electrical isolation and vacuum are maintained using a machined teflon block of a design similar to a conflat.

The chamber is evacuated using two diffusion pumps (one is 0.254 m in diameter and the other is 0.152 m in diameter) operating in parallel. In order to achieve the lowest possible pressures, liquid nitrogen can be supplied to cool the diffusion pumps. Rough pumping is performed by a rotary pump.

Evaporation is achieved using two water cooled, copper crucible, electron beam guns; this allows for the deposition of alloys and multilayer films without venting and opening the chamber. An Airco Temescal Model CV14 power supply, generally operated at 10 kV and between 0.2 and 0.5 Amperes current per gun, powers the electron guns. The use of electrically retractable shutters over each gun prevents the deposition of coating material onto the substrates during the warm up of the evaporation source.

Gases arrive in the chamber via stainless steel tubes. The

flow rates are adjusted using mass flow controllers with delivery rates of 50 or 100 sccm for research purity argon, oxygen, nitrogen and acetylene. Laboratory grade nitrogen is inleted into the chamber through a vent valve in order to raise the system to atmospheric pressure.

A Sloan Model 7 power supply provides up to 7.5 kV and 0.75 amps d.c. to the cathode in order to create and support a glow discharge.

Accessories to the system include a Fluid Precision Instruments capacitance manometer for determination of the pressure in the upper chamber. An Inficon Model 1000 residual gas analyzer (RGA) is used to determine the partial pressures of gas species in the upper chamber. It mainly is used during reactive ion plating by other investigators in this laboratory. The RGA may also be used to leak check the vacuum system by monitoring the amount of helium inlet into the chamber through a leak. A schematic of the ion plating system is shown in figure 3.

B. Experimental Design

Copper and chromium were chosen as evaporant materials and nickel and copper were chosen as substrate materials because of their wide range of solubilities and different crystal structures (FCC coatings on FCC substrates: Cu on Cu and Cu on Ni - complete

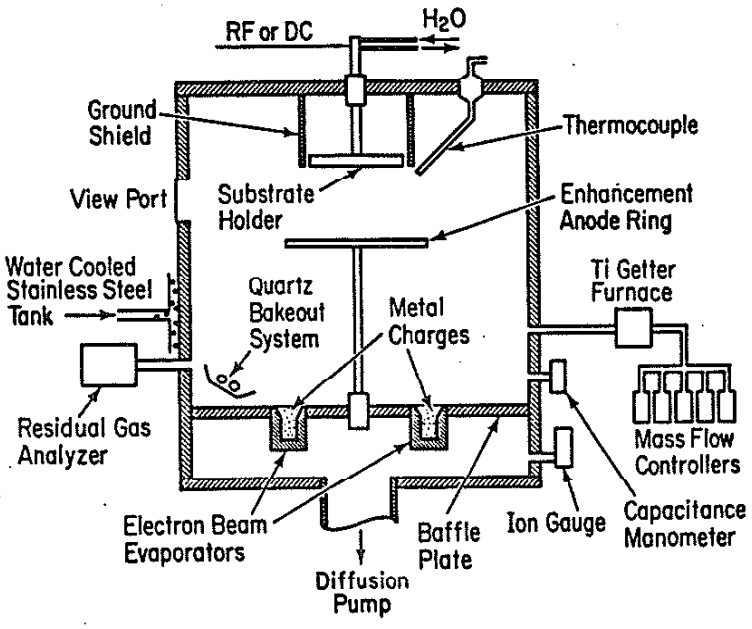

Figure 3 - Schematic of CERL ion plating system

solid slubility; BCC coating on FCC substrate: Cr on Cu - no solid or liquid solubility). The phase diagrams are given in figure 4 and figure 5. The effects of sputter cleaning prior to deposition and substrate bias during deposition on these systems' coating/substrate interfacial regions, coating microstructure and coating properties were selected to be studied in order to gain a more thorough understanding of the fundamentals of the ion plating technique.

The main experimental design was to change one variable at a time while maintaining the other variables constant. The variables studied are prior surface sputter cleaning, ion plating bias and evaporant-substrate solid solubility. Pressure, deposition rate and substrate temperature were constant in these experiments.

The experiment can be divided firstly, by evaporant material (Cu or Cr) on a given substrate (Cu or Ni) and secondly, by plating bias (0 kV, 2.15 kV or 3.5 kV). Lastly, the evaporated coatings (0 kV) can be divided into coatings with and without prior surface sputter cleaning.

The purpose of this experimental design is to allow direct comparison between evaporated and ion plated coatings of copper and chromium. The second advantage of this design is to isolate the effects of sputter cleaning from ion plating bias. Most importantly, this design makes it possible to determine if a graded interface is produced even for materials with no solid or liquid solubilities.

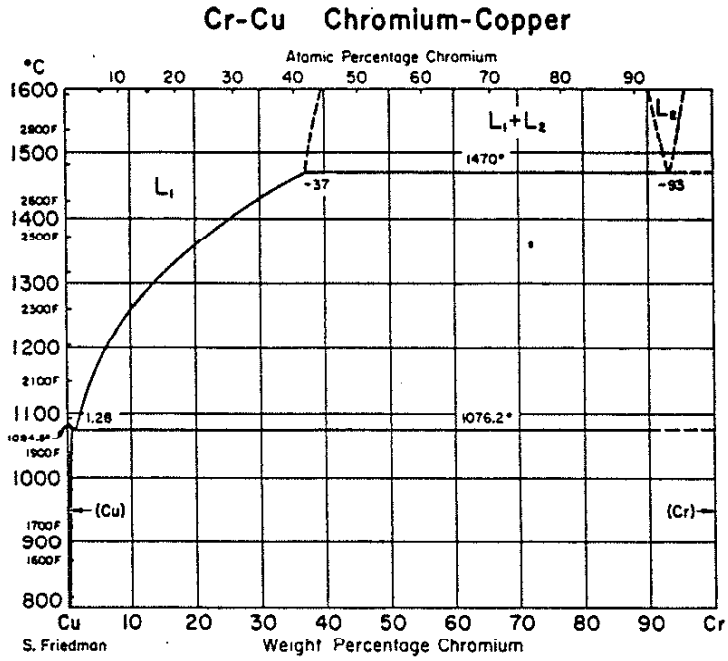

Figure 4 - Chromium-Copper phase diagram

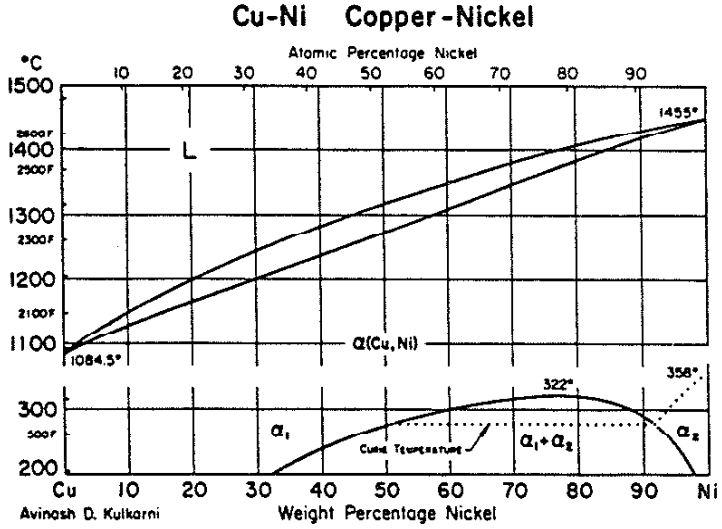

Figure 5 - Copper-Nickel phase diagram

C. Materials Selection

The copper substrate material was oxygen free high conductivity, mildly cold worked sheet with a thickness of 0.075 cm. This material had a 220 orientation as determined by x-ray diffractometry. The grain size was 30 μm.

The nickel was also oxygen free and had a thickness of 0.040 cm. The nickel was in the annealed condition and had a 111 orientation. The grain size was 50 μm.

The substrates were prepared for deposition by mechanically polishing (to 0.25 μm diamond paste) and chemically polishing followed with acetone and ethanol rinses. The chemical polishing solutions are listed in table 1.

The source materials used in this study were 99.9% pure copper and 99.5% pure chromium. These metals were obtained from Aesar, inc. The copper was in shot form (2-5 μm diameter) and the chromium was in chip form. Both materials were consolidated by the electron beam gun.

D. Sample Production

The inside of the upper chamber is covered with aluminum foil prior to deposition in order to reduce cleaning down time. A "dummy deposition" is conducted to coat the upper chamber with the deposition material in order to reduce contamination from backsputtering of the aluminum foil and the stainless steel

Table 1 - Chemical Polishes

Substrate	Solution	Temperature	Time
Copper	33 ml nitric acid 33 ml phosphoric acid 33 ml acetic acid	60-70°C	1-2 min.
Nickel	30 ml nitric acid 10 ml sulfuric acid 10 ml phosphoric acid 50 ml acetic acid	85-95°C	1 min.

chamber. After cooling to 50°C the chamber is vented to affix substrates to the holder. Gloves are worn to prevent contaminating the substrates.

The chamber is evacuated to its base pressure (about 10^{-6} Torr). Then the desired flow rate of the working gas is inlet into the system. If sputter cleaning is desired, the bias to the cathode is applied thus establishing the glow discharge. With the shutters over the crucibles the electron beam is used to slowly heat the source material. When the source is uniformly hot the power of the gun is increased to that desired for deposition and the shutter is opened. When the coating is completed the shutter is closed, the gun turned off and the substrate bias is removed thus extinguishing the glow discharge. The chamber is cooled to 30°C and vented. The specimens are removed and replaced quickly to limit the exposure of the chamber to atmosphere. This minimizes the adsorption of water onto the vacuum chamber walls.

E. Sample Preparation for Analysis

1. Introduction

In order to evaluate the structure, chemistry and properties of the coatings and the coating/substrate interfaces several analytical techniques were performed on the samples. Adhesion testing, x-ray diffractometry and scanning electron microscopy were used to analyze all of the coatings produced. Many of the

coatings were also examined using a scanning Auger microprobe and transmission electron microscopy.

2. Adhesion

The macroscopic bonding of the film to the substrate was determined using a tensile adhesion test. Due to the importance of adhesion and the relative ease of the test adhesion is generally the first test performed on the coating. A Sebastian adherence tester, produced by Quad Group, is used in this study. An epoxy coated aluminum stub is bonded to the coating using a cure temperature of 150°C for one hour. The stub is loaded in tension by the adherence tester. Upon failure the load is removed and the failure stress is displayed in units of psi. The maximum load is 10,300 psi (71 MPa), but the epoxy often fails before this limit is reached.

3. X-ray Diffractometry

Before being sectioned for further investigation the samples were examined with a Norelco x-ray diffractometer using monochromatic Cu kα radiation. This allowed for detection of any preferred orientation.

4. Scanning Electron Microscopy

Both broadface and cross section samples were examined in a

JEOL 35C SEM. The cross sections were prepared by shearing the coating/substrate composite.

5. Scanning Auger Microprobe

A VCR Group Model D400 dimpler (San Francisco, California) was used to mechanically thin samples for depth profiling in a scanning Auger microprobe. The broadface samples were produced using diamond pastes of decreasing grit size (250 nm final size) and the flattening tool. Thinning continued until regions of the substrate were present. This technique was not very successful as the coating was too thick for quick analysis.

6. Transmission Electron Microscopy

Production of TEM cross section samples was tedious. Parallel sections, 2 mm wide, were removed (normal to the coating) with a low speed diamond saw. These sections were wax mounted to a sanding block with the substrate exposed. The substrate was then sanded on SiC paper to a final thickness of 0.625 mm for copper substrates and 0.375 mm for nickel substrates. After the wax was removed the two sections were epoxied together (coating to coating). The combined section was then fitted into a 2.25 mm diameter stainless steel rod with either a 1.25 mm or a 0.75 mm wide slot for mounting the copper and nickel substrates, respectively. The rod was fitted into a 3 mm outside diameter stainless steel tube (the dimension required

for TEM stages) with an inside diameter of 2.35 mm which had just been filled with epoxy. The samples were cured at 50°C for 24 hours. Next, 0.25 mm thick sections were sliced from the rod using a low speed diamond saw. Both sides were mechanically polished, using a VCR dimpler and the flattening tool, with decreasing grit size diamond paste to a final size of 3 μm. The VCR dimpler is equipped with a differential micrometer which allows for controlled removal. Flat polishing of the disks was terminated at 0.120 mm and dimpling begun.

The advantage of dimpling is two fold. Firstly, it provides a sturdy TEM sample as the outer rim remains 0.120 mm thick while the center is thinned to about 1500 nm. Secondly, after thinning a Gatan argon ion miller can be used more effectively for the final thinning. In order to prevent separation of the coating from the substrate, a beam block was used to stop the beam from milling parallel to the coating/substrate interface.

Broadface TEM samples of chromium coatings were made from spalled coatings or coatings removed from the substrate with a razor blade. The coatings were placed in ethanol. The columns were separated from each other by using an ultrasonic cleaner. Copper TEM grids (200 mesh) with a formvar coating were dipped into the ethanol to attach the coating to the grid.

The samples were studied in a Phillip's 400, Phillip's 420 or Phillip's 430 TEM. Bright field imaging, dark field imaging, selected area diffraction and energy dispersive analysis of x-rays (EDAX) techniques were all utilized.

IV. Results

A. Introduction

The results of this study are presented in the following sections. A report of the sputter cleaning rate is presented first, followed by the specimen deposition parameters. The results of each coating system (Cr on Cu, or Cu on Ni) is then presented. The physical properties (thickness and adhesion) of the coating/substrate composite are given. Next X-ray diffraction data of the uncoated substrates and the coatings are presented. The relationships between processing parameters and the coating morphology are detailed through scanning electron microscopy (SEM). Transmission electron microscopy (TEM) data concerning the structure and chemistry of the coating and coating/substrate interface are then presented. Lastly, surface chemical data and chemical composition vs. depth profiles obtained from a scanning Auger microprobe are reported.

B. Sputter Rate

The effect of cathode bias on the rate of sputter removal durring sputter cleaning was examined. The samples had identical preparations, described earlier, (mechanical polishing and chemical polishing) as the substrates used for the rest of the experiments. The sputtering conditions are given in table 2.

Table 2 - Sputter Rate Data

Material	Time (min)	Pressure (mTorr)	Bias (kV)	Sputter Rate * atoms/cm^2sec
Cu	60	5.0	1.50	1.17×10^{14}
Cu	60	5.0	2.25	3.99×10^{14}
Cu	60	5.0	3.50	6.99×10^{14}
Ni	60	5.0	1.50	2.52×10^{13}
Ni	60	5.0	2.25	6.42×10^{13}
Ni	60	5.0	3.50	3.34×10^{14}

* Calculated from weight loss

The sputter removal rate, calculated from weight loss, is approximately equal to half of a monolayer per second. Thus for a typical sputter cleaning time of 10 minutes, 300 monolayers or about 1000 Å (0.10 μm) of material is removed. This is why sputter cleaning is said to provide a nearly atomically clean surface for coating. The coating material deposition flux must exceed this rate in order for net film growth to occur.

C. Specimen Parameters

The sample production conditions which were varied in this experiment are recorded in table 3. The independent variables for a particular coating/substrate system (Cr on Cu or Cu on Ni) were sputter cleaning and applied substrate bias durring deposition. All other processing parameters were held as constant as possible (the only exception is for the non-sputter cleaned chromium coating for which the current of the electron beam gun was double that of the other chromium coatings. The sample production conditions, which were not varied, are reported in table 4.

D. Chromium on Copper Substrates

Four chromium coatings were produced on copper substrates. The coating evaluation and processing parameters are listed in tables 3 and 4, respectively. Two were produced with no substrate bias during deposition, of these only one underwent

Table 3 - Chromium Coating Specimen Parameters

Sample	Deposition Rate (A/sec)	Thickness (μm)	Bias (kV)	Sputter Clean	Failure Load (psi)	Failure Locus
1	115.6	20.8	--	No	Spalled	Cr/Cu
2	46.2	8.3	--	Yes	2050	Cr
3	44.7	8.0	2.15	Yes	5770	Cr
4	42.1	7.8	4.00	Yes	2970	Cr/Cu

Table 4 - Processing Parameters

Base pressure			: $1x10^{-6}$ Torr
Sputter cleaning*		time	: 10 min
		bias	: 3.0kV
		pressure (Ar)	: $5x10^{-3}$ Torr
Evaporation		time	: 30 min
		pressure (Ar)	: $5x10^{-3}$ Torr
		bias	: 10 kV
	Chromium	current	: 0.40 A**
		current	: 0.20 A
	Copper	current	: 0.60 A
Substrate bias*		voltage	: 0 - 4.0 kV

* Independent variable

** The non-sputter cleaned chromium coating was evaporated with 0.40 A current. The other chromium coatings were produced with 0.20 A current.

NOTE: The substrate holder is water cooled. The temperature, as measured with a thermocouple placed in the glow, was below 250°C.

substrate sputter cleaning prior to deposition. The other two had substrate sputter cleaning and substrate biases of 2.15 kV and 4.0 kV durring deposition. The thickness, adhesion, structure and chemistry of the coatings and coating/substrate interfaces are reported in the following subsections.

1. Thickness

The average thickness of the coatings was measured on cross-sectioned samples using SEM and is reported in table 3. The evaporated coating with no sputter cleaning was the thickest (20.8 μm). The thickness decreased throughout the rest of the series (evaporated with sputter cleaning: 8.3 μm; 2.15 kV ion plated: 8.1 μm and 3.5 kV ion plated: 7.6 μm). The evaporation time was constant for all the coatings (30 min). However, the current to the electron beam gun for the for the non-sputter cleaned sample (0.40 A) was double the current for the rest of the coatings. It is apparent from the similar thicknesses of the last three coatings that good coating thickness control is possible by evaporation even for an element like chromium which sublimes.

2. Adhesion

The adhesion data and the locus of failure of the chromium coatings is given in table 3 along with the specimen parameters. Note that two of the samples failed in the coating and two failed

at the interface. Three major results are evident. Firstly, sputter cleaning the substrate prior to deposition increases the adhesion strength of the evaporated coatings from essentially zero (for the non-sputter cleaned sample) to 2050 psi (for the sputter cleaned sample). Secondly, increasing the bias durring deposition from zero to 2.15 kV also increases the adhesion strength (to 5770 psi). Lastly and unexpectedly, a further increase in coating bias (to 4.0 kV) causes a decrease in the adhesion strength (to 2970 psi).

3. X-ray Diffractometry

X-ray diffractometry data was collected from each of the samples. Table 5 summarizes integrated intensity ratios of the copper substrates and the chromium coatings. According to the x-ray powder diffraction files a random powder of chromium will have the Cr(110) peak as the strongest with the Cr(200), Cr(211) and Cr(220) having 16%, 30% and 18% of the Cr(110) integrated intensity. The chromium coatings were grown on copper substrates with a (220) orientation. The orientations of the evaporated coatings (with and without sputter cleaning) are similar as both have a nearly random Cr (110) orientation. These are the most densely packed planes in the bcc structure but are not significantly denser than several other planes. The use of plating bias has a marked effect on the grain orientation. Use of a 2.15 kV plating bias causes a change in preferred orientation to the Cr(200) planes and this coating has a

Table 5 - X-ray Diffractometry of Cr Coatings on Cu Substrates

Sample	Sputter Cleaning	Plating Bias	Relative Intensity			
			(111)	(200)	(220)	(311)
Cu Substrate	--	--	16.0	47.6	100.0	38.8
Cu Powder	--	--	100.0	46.0	20.0	17.0
			(110)	(200)	(211)	(220)
1	No	No	100.0	11.6	23.2	5.6
2	Yes	No	100.0	7.9	11.8	0.0
3	Yes	2.15	35.0	100.0	11.1	1.5
4	Yes	4.00	0.0	100.0	0.0	0.0
Cr Powder	--	--	100.0	16.0	30.0	18.0

Cr(200)/Cr(110) intensity ratio of 100/35. Increasing the bias increases the preferred orientation so much that only the Cr(200) planes produce significant diffracted intesity.

4. Scanning Electron Microscopy

Scanning electron microscopy was used to relate the coating morphology to the independent processing parameters. Figures 6-9 reveal much about the effect of sputter cleaning and substrate bias durring coating. The evaporated chromium coating without sputter cleaning (figure 6) has an open columnar, zone 1, structure with domed tops. The use of sputter cleaning alters the morphology of the coating by making the columns pack more densely and making them less well defined (figure 7). This is typical of a zone T morphology. The application of a 2.15 kV ion plating bias causes a change to a zone 2 morphology which is characterized by well-defined densely packed columns with faceted tops (figure 8). Increasing the ion plating bias to 4.0 kV produces loosely packed, extremely well-defined faceted columns with square based pyramidal faceted tops (figure 9). This morphology is consistent with the preferred orientation revealed in the x-ray diffractometry data. This morphology (open columns with faceted tops) allows the coating to absorb light from nearly any angle (except grazing angles).

The SEM yields information on the coating morphology but does not supply the information about the coating/substrate interface necessary to understand the adhesion data. Examination of the

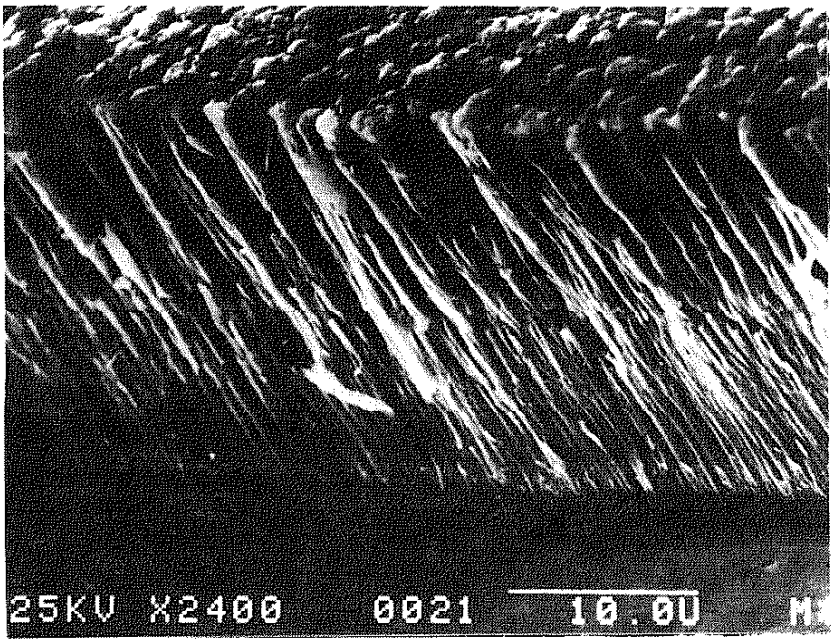

Figure 6 - SEM of evaporated chromium sample on non-sputter cleaned copper substrate

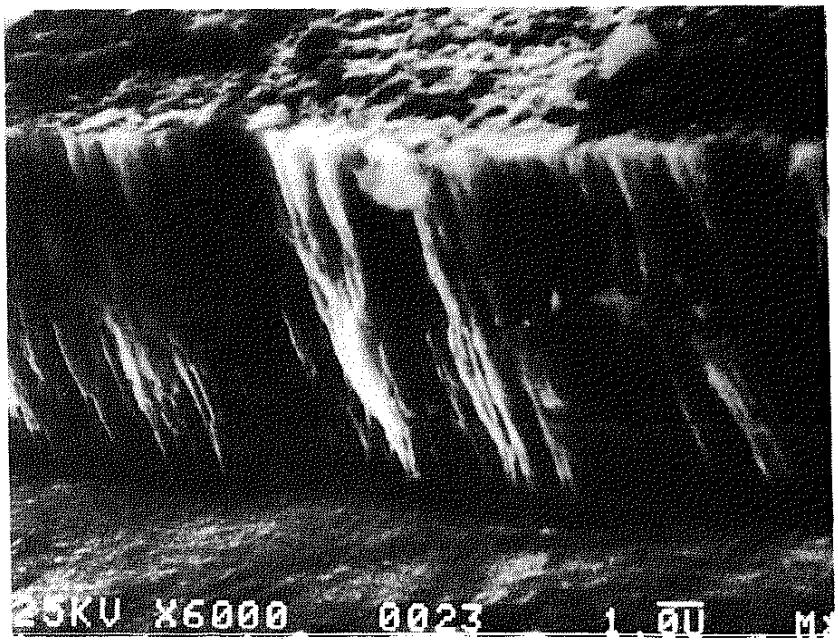

Figure 7 - SEM of evaporated chromium sample
on sputter cleaned copper substrate

Figure 8 - SEM of 2.15 kV bias ion plated chromium sample on sputter cleaned copper

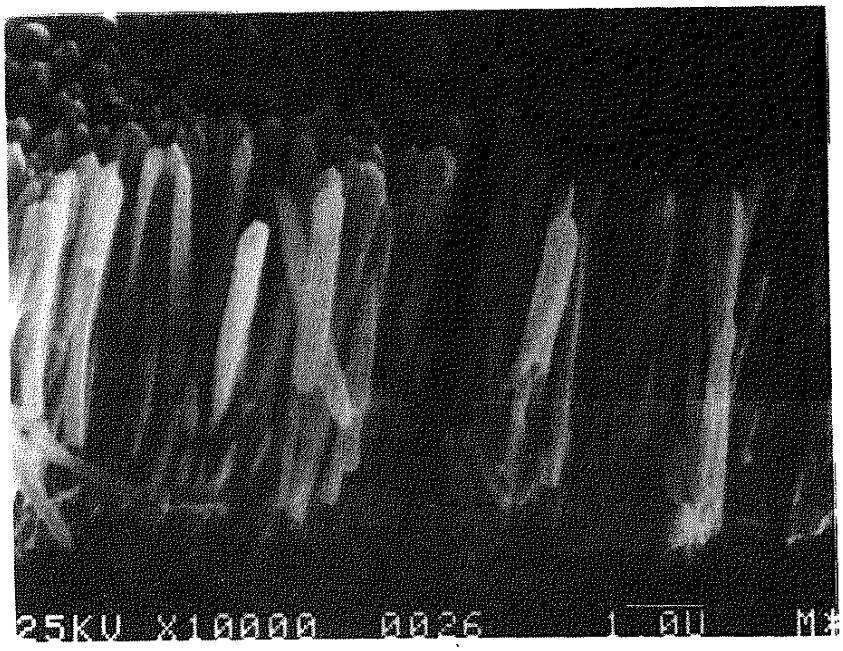

Figure 9 - SEM of 4.00 kV bias ion plated chromium sample on sputter cleaned copper

interface is needed and is accomplished using cross-section TEM and scanning Auger depth profile analysis.

5. Transmission Electron Microscopy

Interface study using TEM is one of the primary tools used in this research as it is believed that the structure and chemistry of the interface determines the adhesion properties of the coating/substrate composite. Figures 10-20 comprise the TEM and EDX analysis of chromium coatings #2-#4. No cross section TEM samples of the non-sputter cleaned, evaporated coating (#1) could be produced due to its poor adhesive strength.

Figure 10 is a bright field micrograph of the evaporated chromium coating with prior sputter cleaning (#2) and shows a 300 Å wide dark layer adjacent to the coating/substrate interface. The dark-field micrograph (figure 11) shows the polycrystalline nature of the coating and a microcrystalline, dense layer in the coating near the interface before well-defined columnar growth begins. EDX analysis (figures 12 and 13) of this coating shows no mixing of the coating (chromium) and the substrate (copper) elements at distances as small as 100 Å from the interface. Small amounts of copper and chromium are present all over the TEM sample due to sample preparation methods (mechanical polishing and ion milling). The dark layer, therefore, is believed to be a sputter cleaning induced damaged layer in the substrate. The coating is dense for the first 800 Å before transforming to a columnar morphology. Figure 14 is a

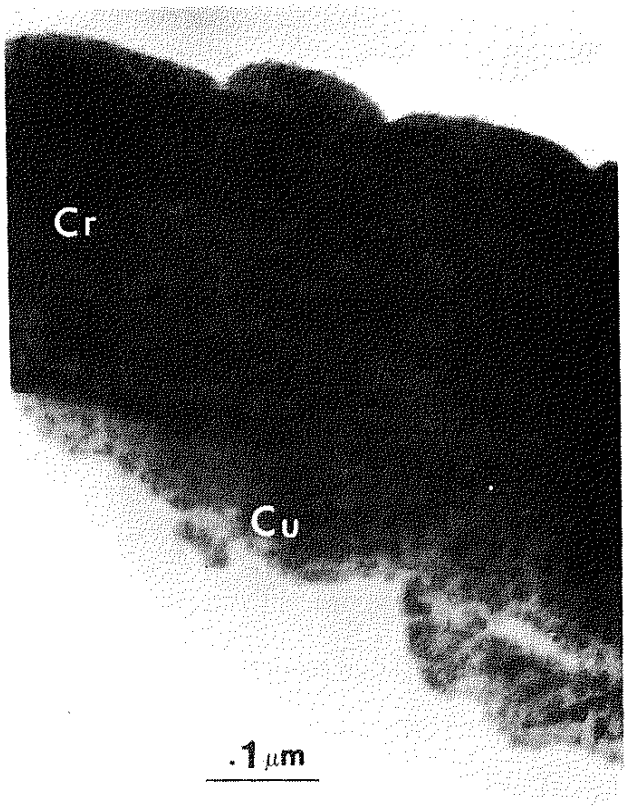

Figure 10 - TEM micrograph of evaporated chromium film on sputter cleaned copper (bright field)

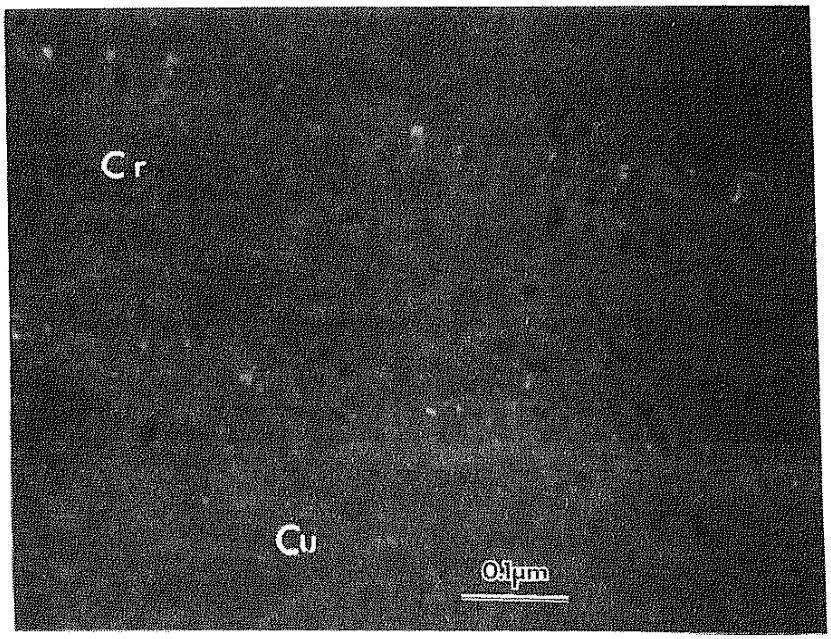

Figure 11 - Dark field corresponding to figure 10

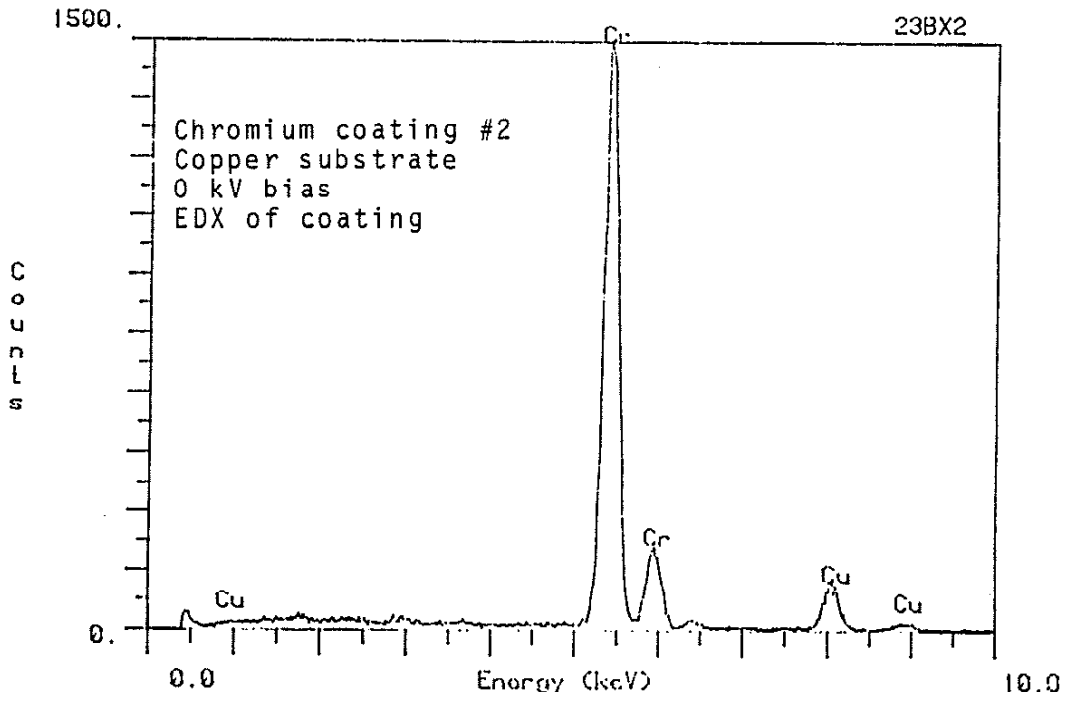

Figure 12 - EDX scan of evaporated chromium film on sputter cleaned copper 200 Å from the interface

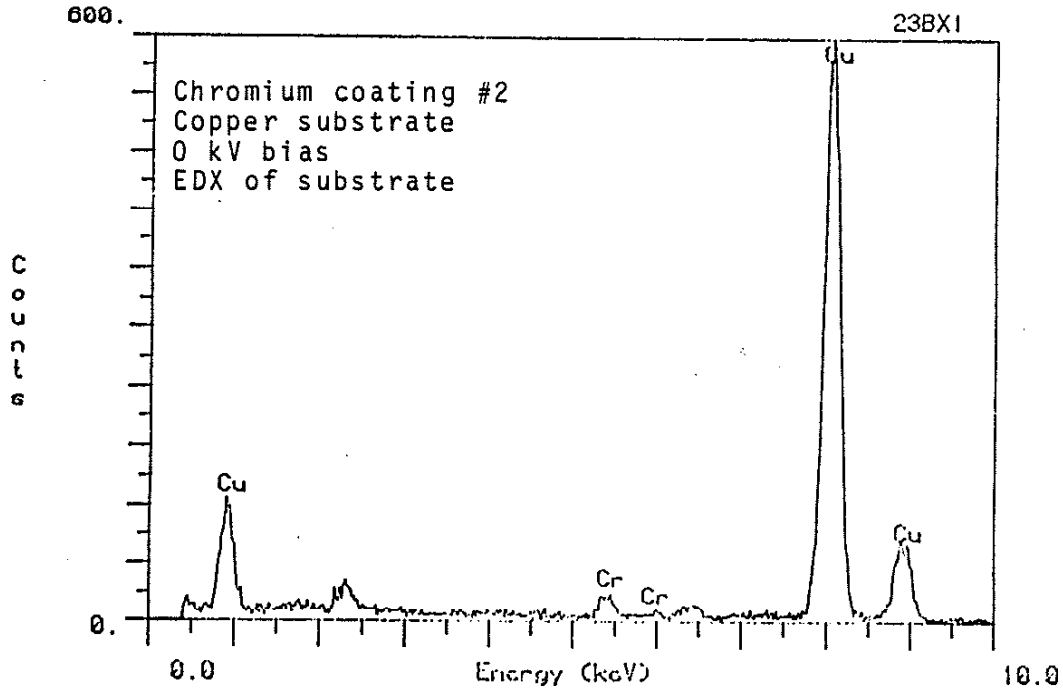

Figure 13 - EDX scan of copper substrate corresponding to figure 12, 200 Å from the interface

selected area diffraction pattern from the coating showing its polycrystalline nature. Table 6 identifies the crystallographic planes corresponding to the rings. All of the chromium coatings (including the ion plated coatings) exhibit similar rings in the diffraction patterns.

Figures 15-20 represnt the TEM and EDX analysis of 4.0 kV bias ion plated chromium coating on sputter cleaned copper (#4). Figure 15 shows the columnar nature of the coating. Some separation of the columns is also evident. It also shows two layers at the interface. The layer in the substrate is approximately 300 Å thick while the layer in the coating is about 400 Å thick. The dark field micrograph (figure 16) shows the layer in the coating has very little crystalline nature and is possibly amorphous. This coating is columnar starting from the 400 Å wide layer and throughout the coating, having no microcrystalline component. EDX analysis of this coating (figures 17 and 18) shows chemical mixing on both sides of the interface as copper is present in the coating a significant distance from the interface (0.1 μm). Likewise, chromium is found in large concentrations even 800 Å into the substrate. Figures 19 and 20 show a single unthinned column of this coating which was detatched from the substrate with a razor blade and attached to a copper TEM grid. A central spine is evident as are secondary growth arms extending from the spine. This structure is typical of dendritic growth. The dark field readily shows the column is made of many finely sized (about 600 Å diameter) crystals.

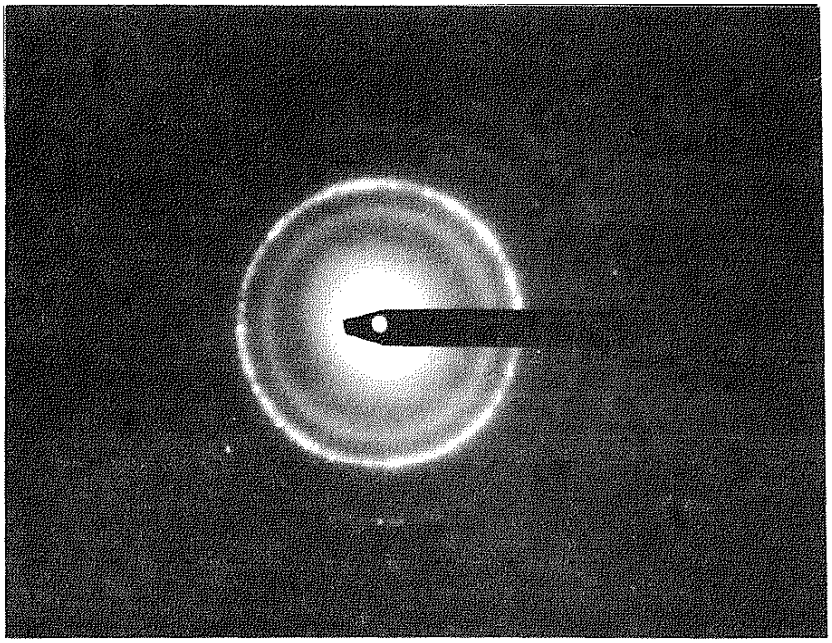

Figure 14 - Selected area diffraction pattern from evaporated chromium film on sputter cleaned copper

Table 6 - Chromium Electron Diffraction Pattern Analysis

Ring Number	Chromium Crystallographic Plane
1	*
2	110
3	200
4	211
5	220

* amorphous ring

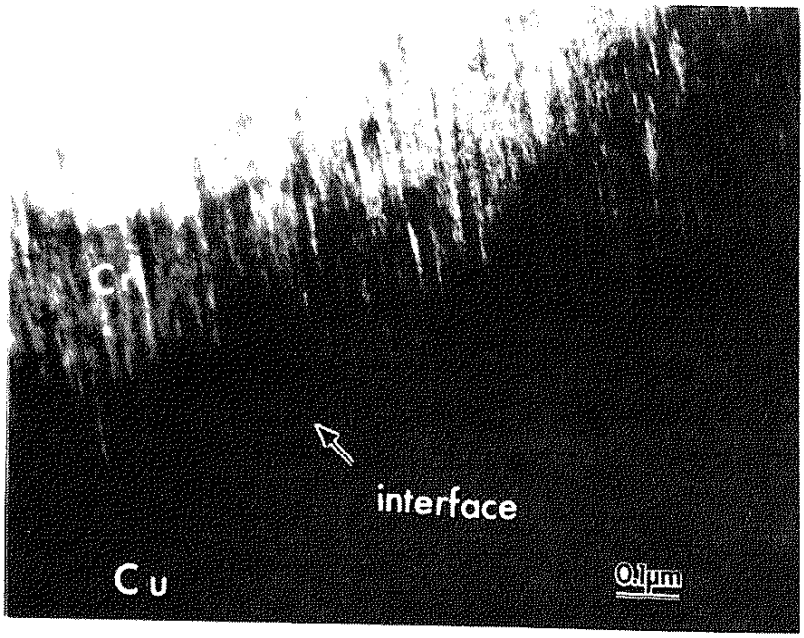

Figure 15 - TEM of 4.0 kV bias ion plated chromium film on sputter cleaned copper substrate (bright field)

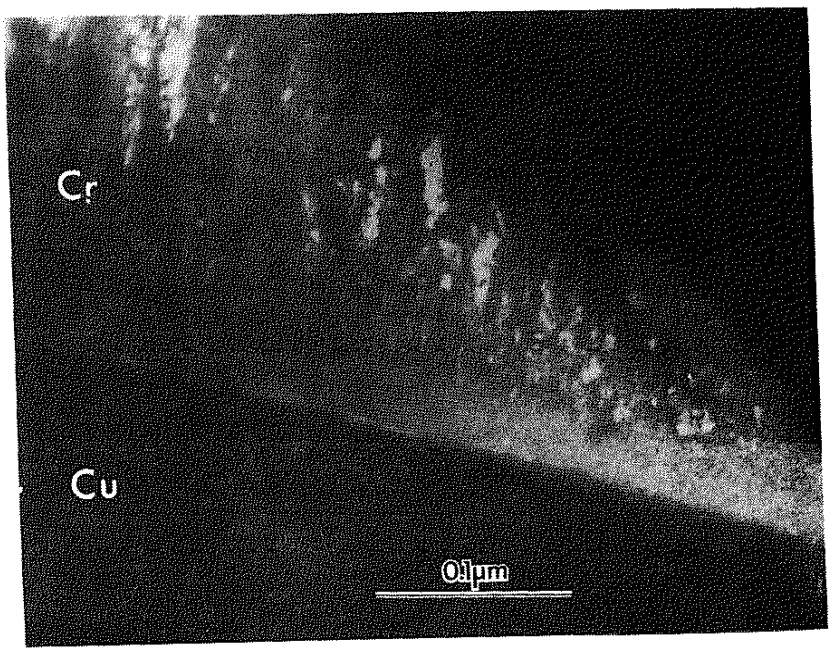

Figure 16 - Dark field corresponding to figure 15

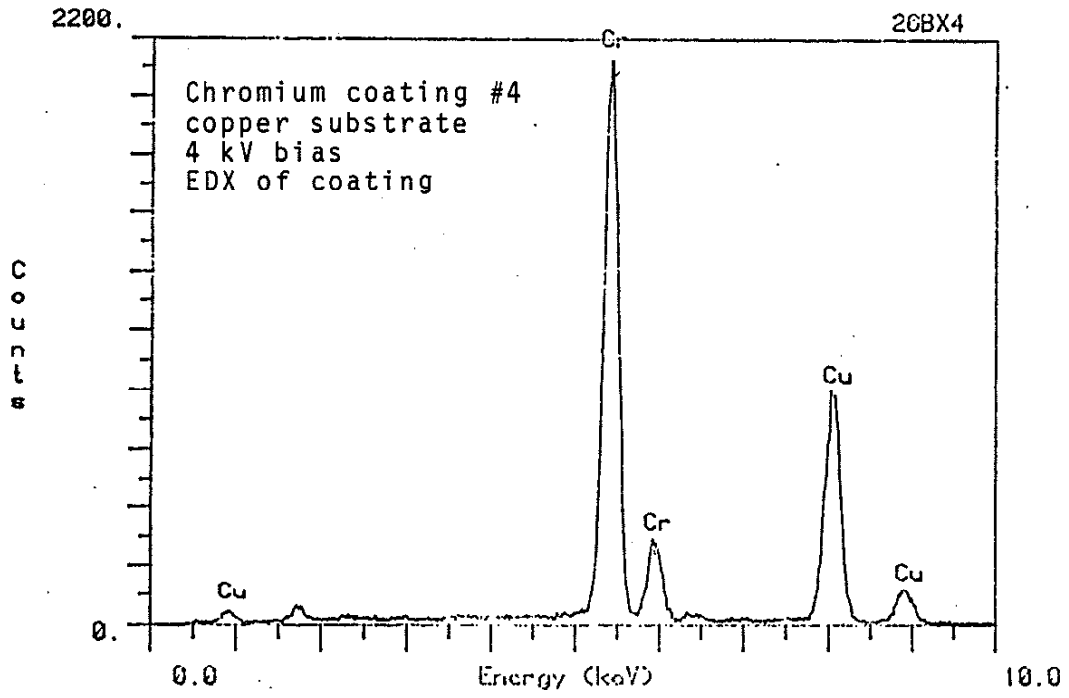

Figure 17 - EDX scan of 4.0 kV ion plated chromium film on sputter cleaned copper 0.1 μm from the interface

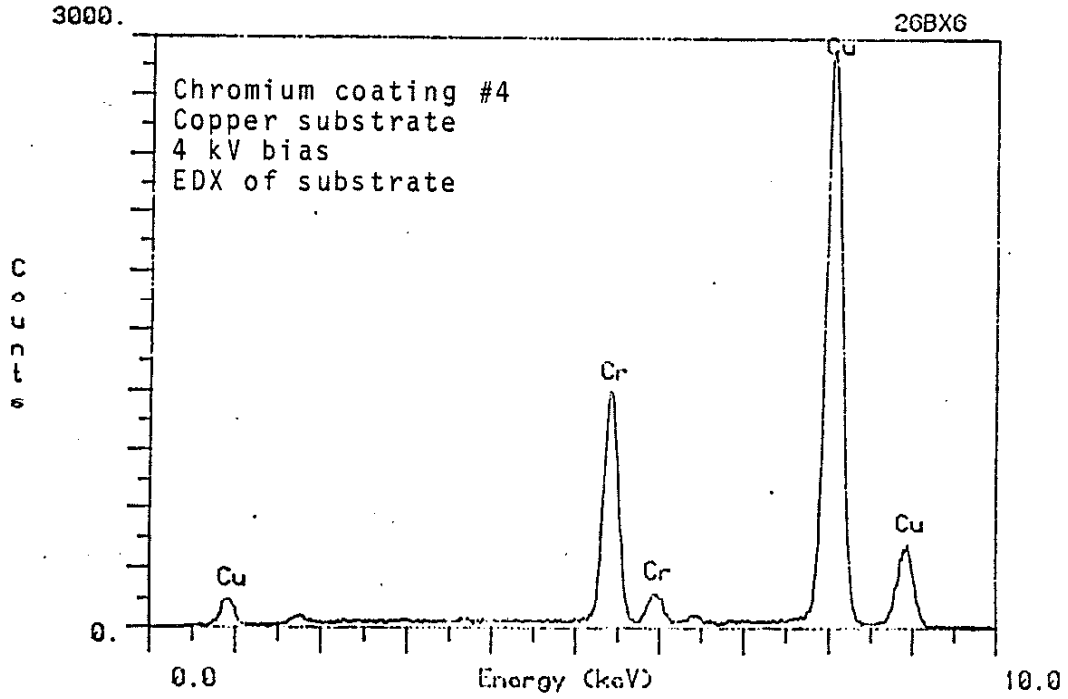

Figure 18 - EDX scan of copper substrate corresponding to figure 17, 800 Å from the interface

Figure 19 - TEM of a single column of the 4.0 kV ion plated chromium coating (bright field)

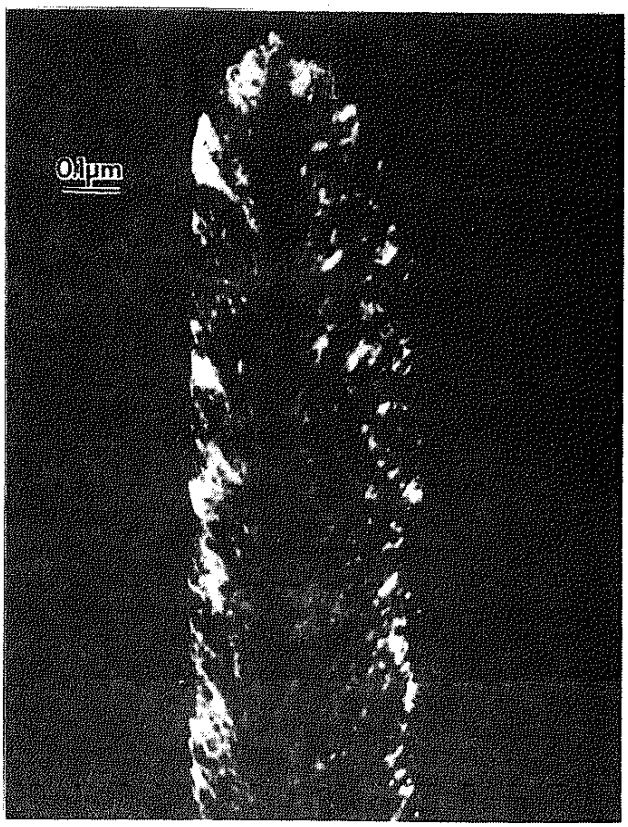

Figure 20 - Dark field corresponding to figure 19

The 2.15 kV bias ion plated chromium coating also has two layers adjacet to the interface as seen in TEM micrographs (not presented here). The layer in the substrate is approximately 300 Å wide and the layer in the coating is also about 300 Å wide. The coating is fully dense and equiaxed for the first 700 Å before changing to a columnr morphology.

6. Auger Analysis

Auger depth profiling was performed on all chromium coating adhesion samples after failure. This allows one to determine the actual locus of failure. For the evaporated chromium coating without sputter cleaning (#1) no chromium is detected by Auger electron spectroscopy (AES) on the atmosphere exposed copper substrate after removal of the chromium coating by the adhesion test (figure 21). These results show that the failure, therefore, occurs at the coating/substrate interface and this interface is chemically sharp.

For the evaporated coating with sputter cleaning (#2) no copper is found in the detached coating (figure 22), but chromium is still present on the substrate (figure 23). Thus the adhesion failure occurs within the coating and not at the coating/substrate interface. Sputter depth profiling to the interface takes 9 minutes (figure 24). The sputter rate is approximately 1 μm/hr. This means that approximately 0.15 μm of chromium coating is attached to the substrate. Sputtering through the interface requires 21 minutes and corresponds to an

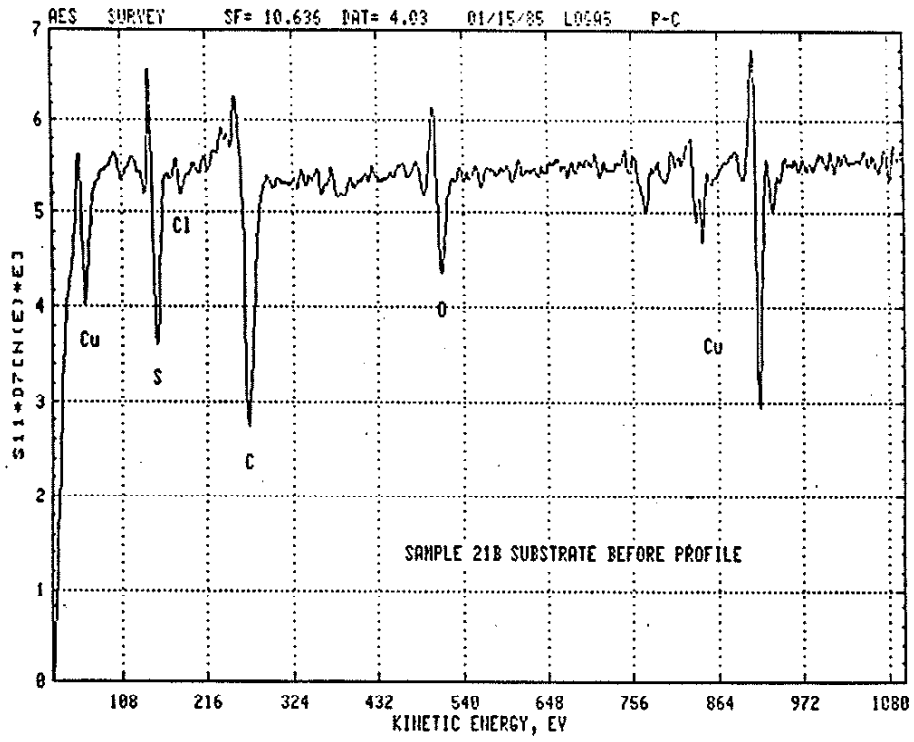

Figure 21 - Auger surface survey of adhesion substrate of evaporated chromium coating produced without prior copper substrate sputter cleaning

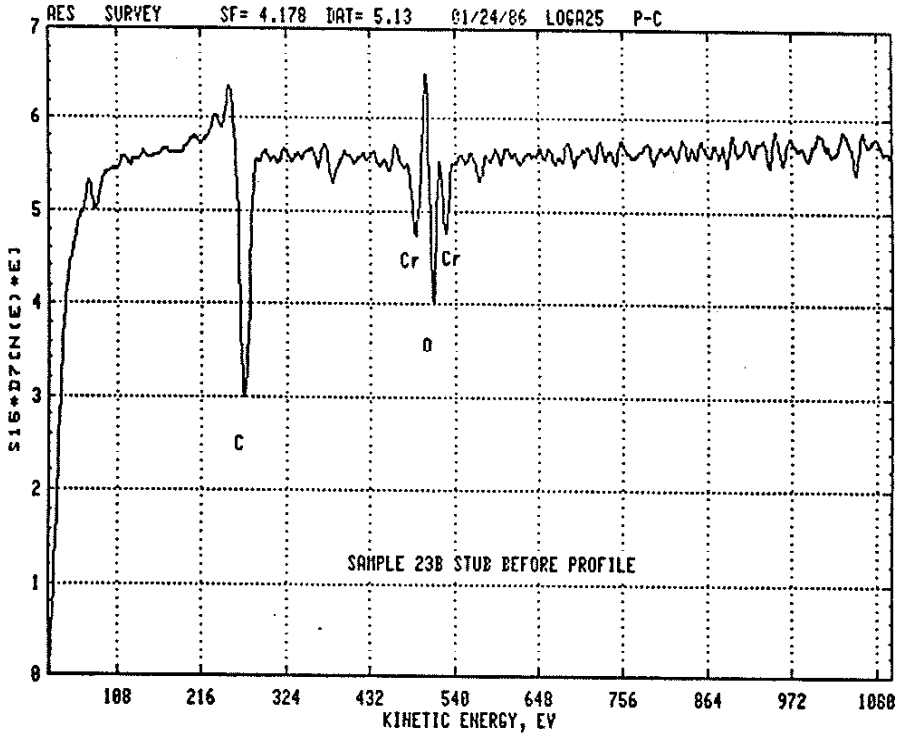

Figure 22 - Auger surface survey of adhesion pull stub of evaporated chromium film produced with prior copper substrate sputter cleaning

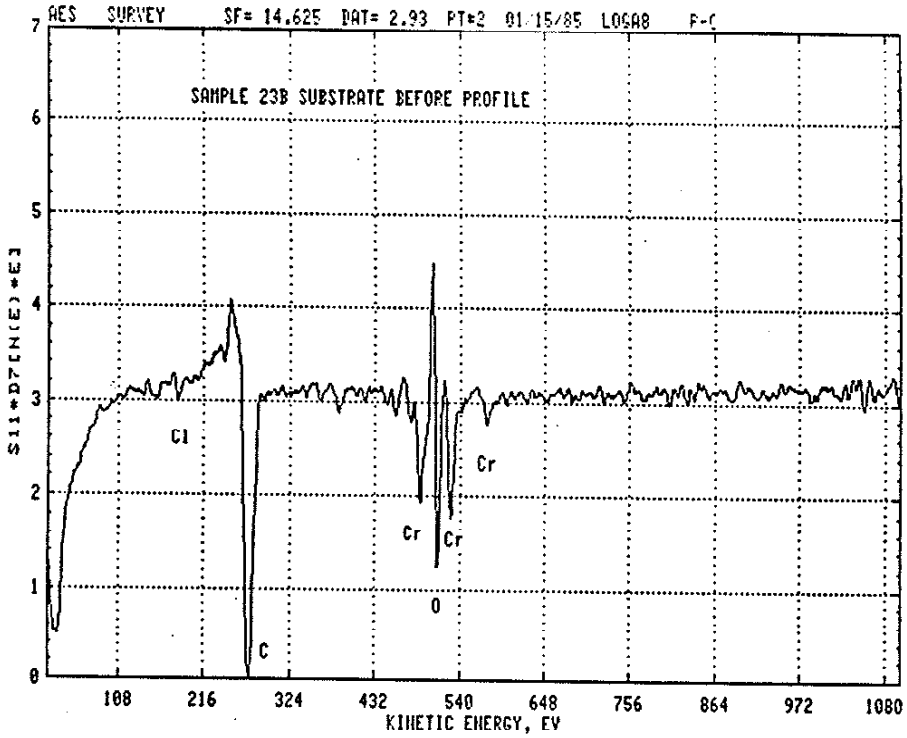

Figure 23 - Auger surface survey of adhesion substrate of evaporated chromium film produced with prior copper substrate sputter cleaning

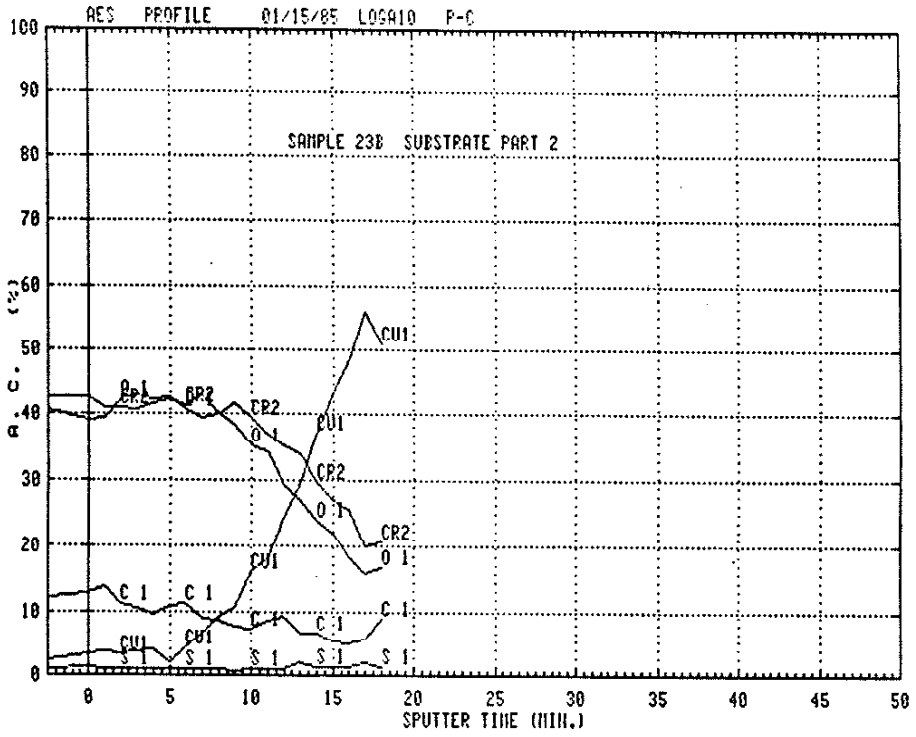

Figure 24 - Auger depth profile of adhesion substrate of evaporated chromium film produced with prior copper substrate sputter cleaning

interface about 0.35 μm wide. No chemical mixing was evident in the TEM EDX analysis, however.

The 2.15 kV ion plated chromium sample (#3) also failed in the the coating near the interface (figure 25). Sputtering to the interface takes 10 minutes (0.17 μm) and through the interface requires 55 minutes (0.92 μm).

The 4.0 kV ion plated chromium sample (#4) fails at the coating/substrate interface as copper is evident in the chromium removed from the substrate (figure 26), but no chromium is present in the substrate (figure 27). This coating had a lower adhesion strength than the 2.15 kV ion plated coating. Sputtering into the chromium through the interface (figure 28) takes only 14 minutes (about 0.23 μm) which is consistent with TEM EDX analysis result of a 0.18 μm wide interface. The Auger analysis also reveals that oxygen contamination occurs in each of the chromium coatings. Note that the depth profiles are reported using peak to peak data and not concentrations. Also AES is highly sensitive to oxygen and the oxygen and chromium peaks overlap causing the apparently high oxygen levels in the depth profiles.

Sputter depth profiling also was perfomed on two chromium coatings thinned using a dimpler and the flattening tool until the coating was totally removed in some areas. The Auger sputter depth profiling was done in the coating ajacent to the exposed substrate region. The evaporated coating with substrate sputter cleaning takes about 18 minutes to sputter through the the interface (figure 29). This corresponds to a 0.30 μm wide

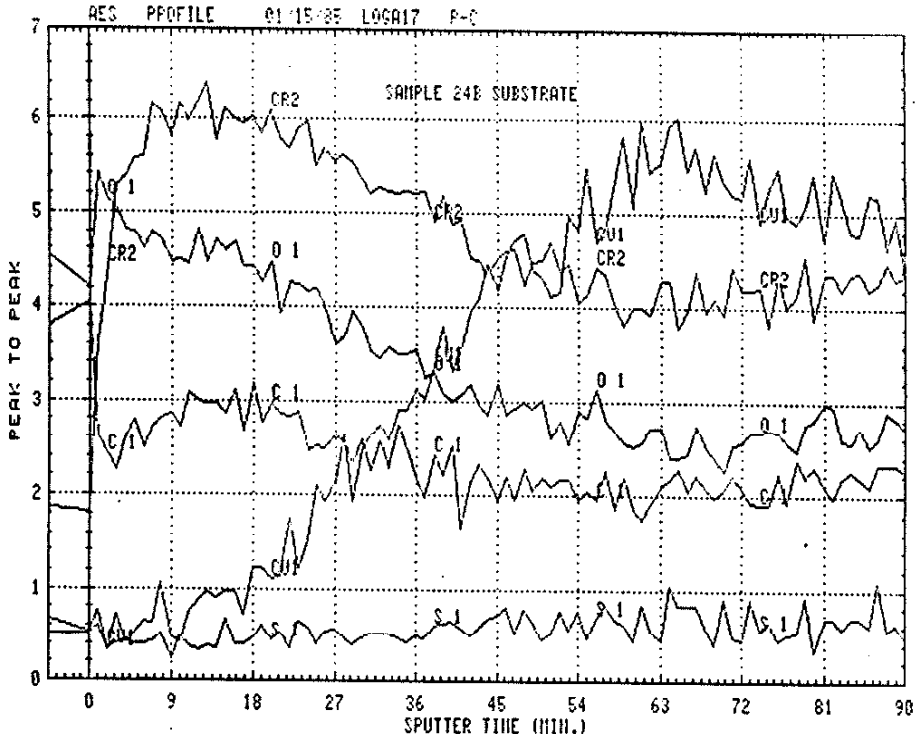

Figure 25 - Auger depth profile of 2.15 kV bias ion plated chromium coating on a sputter cleaned copper substrate (substrate of adhesion test)

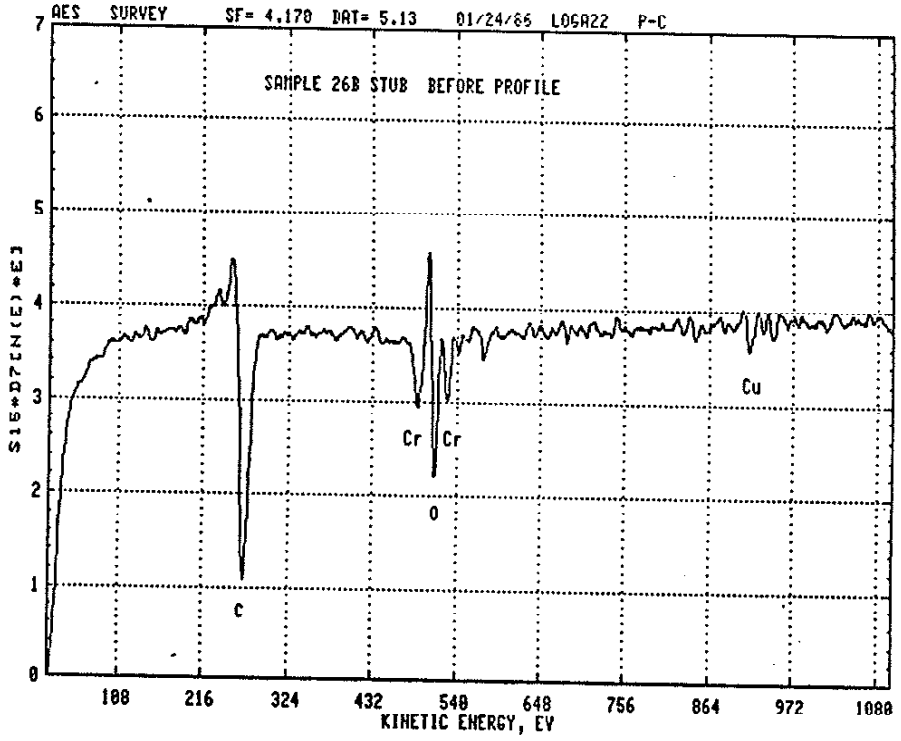

Figure 26 - Auger surface survey of 4.0 kV bias ion plated chromium film on adhesion pull stub

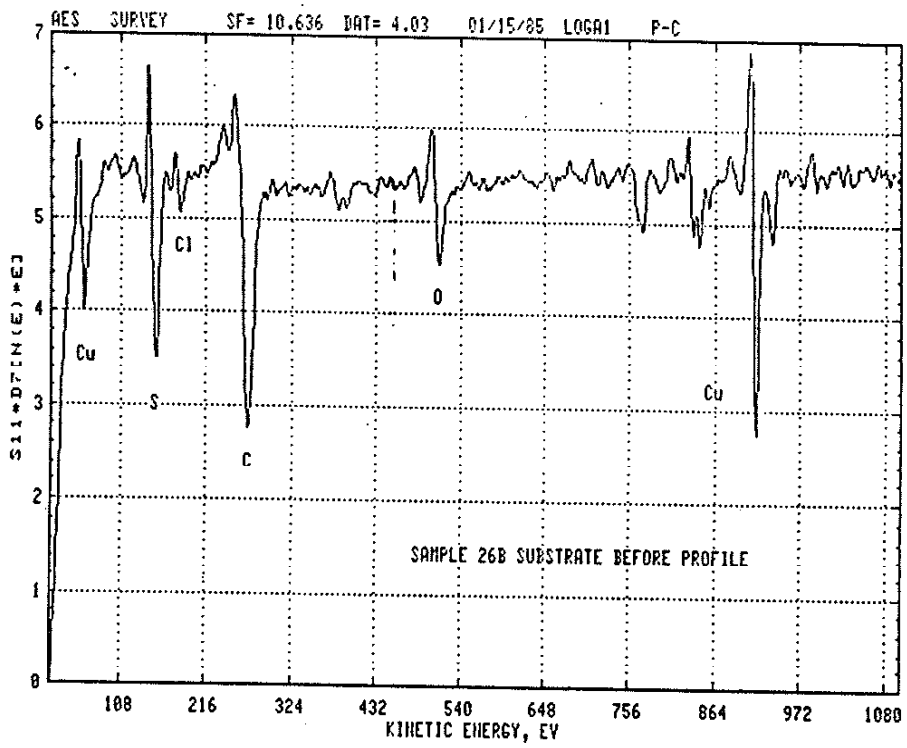

Figure 27 - Auger surface survey of adhesion substrate of 4.0 kV ion plated chromium film on a copper substrate

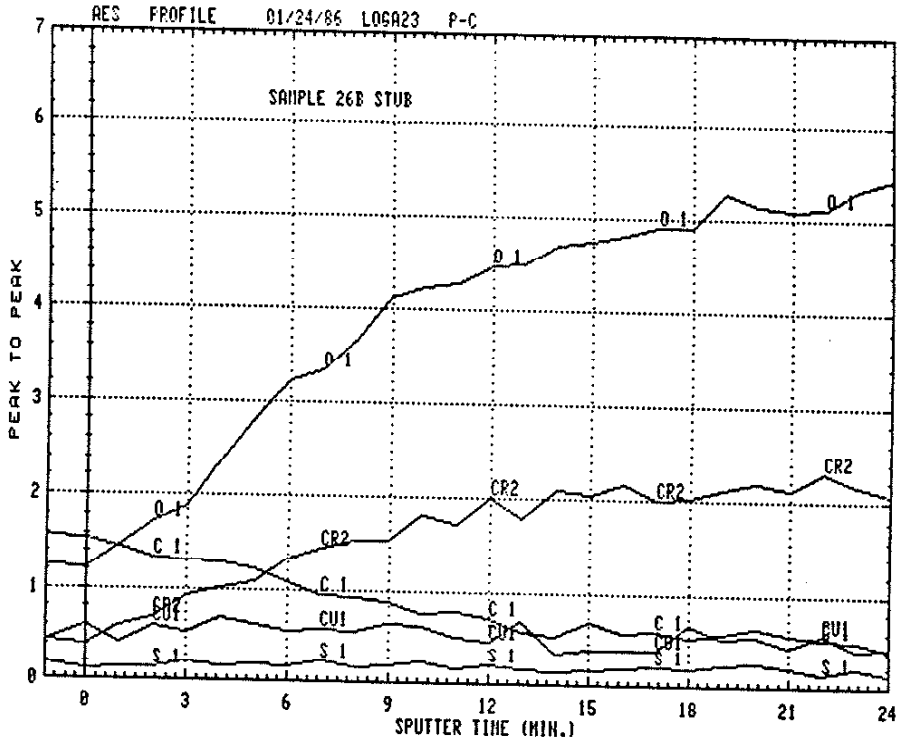

Figure 28 - Auger depth profile of 4.0 kV bias ion plated chromium coating on a sputter cleaned copper substrate (substrate of adhesion test

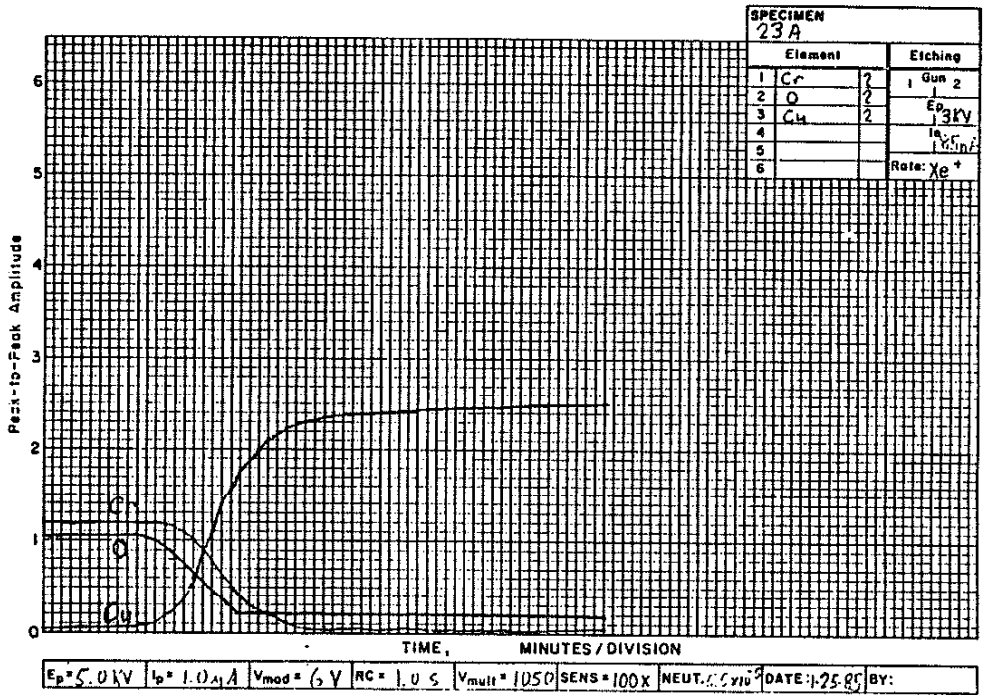

Figure 29 - Auger depth profile of mechanically thinned evaporated chromium coating produced on a sputter cleaned copper substrate

interface. The 4.0 kV ion plated sample was also examined. The thinned regions of this coating were too thick for easy examination and required two hours of sputtering before the interface was reached. This may have caused mixing and topographical problems (such as cone formation) and may cause the interface depths to be reported larger than they actually are. The interface is about 1.7 μm wide (100 minutes of sputtering) as determined by this method (figure 30) which is eight times larger than that determined by the Auger study of the adhesion sample and 10 times larger than that determined from TEM/EDX analysis.

E. Copper Coatings on Nickel and Copper Substrates

Four copper coatings were produced on nickel substrates. The specimen parameters are listed in table 7. Two had no substrate bias durring plating, of these only one had substrate sputter cleaning prior to deposition. The other two coatings had substrate sputter cleaning and substrate biases during deposition of 2.15 kV and 3.5 kV. The thickness, adhesion, structure and chemistry of the coatings and coating/substrate interfaces are reported in the following subsections.

1. Thickness

The average thickness of the copper coatings was measured via TEM because the copper was too ductile to make fracture cross-section SEM samples. The evaporation time (30 min) and current

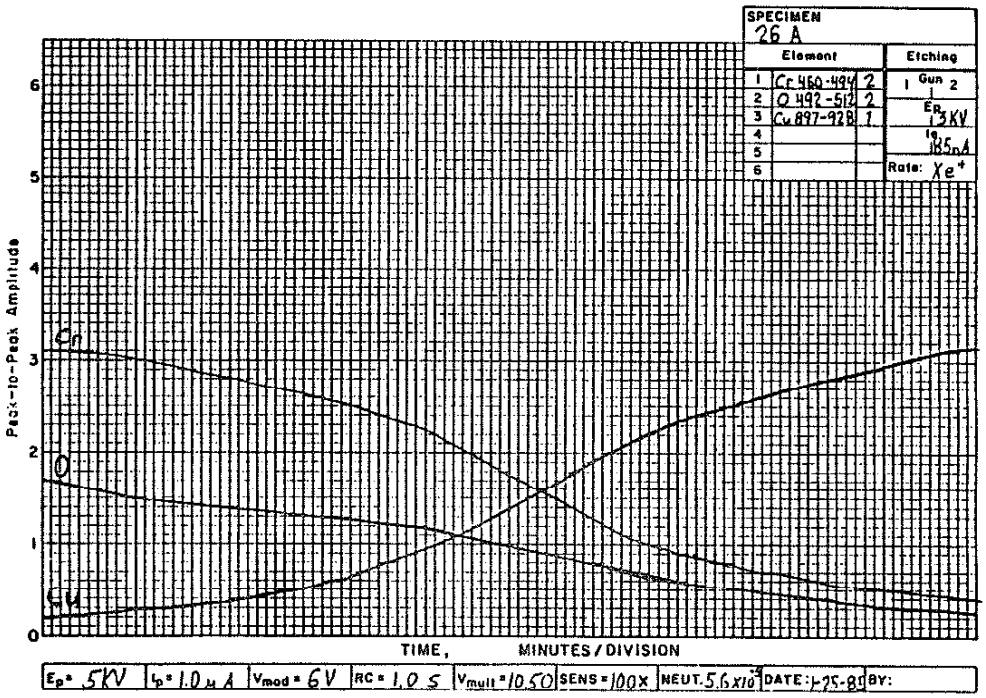

Figure 30 - Auger depth profile of mechanically thinned 4.0 kV bias ion plated chromium coating on a sputter cleaned copper substrate

Table 7 - Copper Coating Specimen Parameters

Sample	Deposition Rate (A/sec)	Thickness (μm)	Bias (kV)	Sputter Clean	Failure Load on Ni (psi)	Failure Load on Cu (psi)
5	51.7	9.3	--	No	Spall	5,620
6	47.3	8.5	--	Yes	1720	6,130
7	41.4	7.4	2.15	Yes	5150	10,200
8	38.3	6.9	3.50	Yes	6520	10,300*

* This sample did not fail. The load limit of the adhesion tester is 10,300 psi.

to the electron beam gun (0.6 A) were constant for all of the copper coatings. The thicknesses and deposition rates are repoted in table 7. The thickness is greatest for the evaporated coating with no sputter cleaning (9.3 μm) and decreases throughout the the series of copper coatings (evapoated coating with sputter cleaning: 8.5 μm; 2.15 kV bias ion plated coating: 7.4 μm and 3.5 kV bias ion plated coating: 6.9 μm)

2. Adhesion

The adhesion and the locus of failure of the copper coatings is listed in table 7 with the specimen parameters. All of the samples which failed appeared to have failed at the coating/substrate interface. Three major results are evident. Firstly, The evaporated copper coating with no sputter cleaning has poor adhesion on nickel (it spalled off) while on copper it had a strength of 5620 psi. Secondly, sputter cleaning improves adhesion on both substrates (1720 psi on nickel and 6130 psi on copper). Use of a glow discharge and a 2.15 kV ion plating bias greatly improves the adhesion (to 5150 psi on nickel and 10,200 psi on copper). Thirdly, increasing the plating bias to 3.5 kV causes a further improvement in adhesion strength to 6520 psi on nickel and greater than 10,300 psi on copper (this sample did not fail as 10,300 psi is the load limit of the adhesion tester used).

3. X-ray Diffractometry

X-ray diffractometry data was collected for each of the copper coatings. Table 8 summarizes the integrated intensity ratios of the nickel substrate and the copper coatings. According to the X-ray powder diffraction files a random copper powder has the Cu(111) peak strongest with the Cu(200), Cu(220) and Cu(311) peaks having 46%, 20% and 17% of the Cu(111) integrated intensity. The copper coatings were grown on nickel substrates with a (111) orientation. All of the copper coatings have a nearly random orientation with the (111) planes having the greatest intensity. The evaporated copper coating without sputter cleaning has a Cu(111)/Cu(200) intensity ratio of 100/88. The sputter cleaned evaporated copper coating has a value of 100/34 for this ratio. The use of a 2.15 kV ion plating bias causes this ratio to increase to 100/18. An increase in the plating bias to 3.5 kV reduces the ratio to 100/32. Thus sputter cleaning and plating bias slightly favor the Cu(111) orientation which also happens to be the substrate orientation.

4. Scanning Electron Microscopy

Scanning electron microscopy was used to relate the coating morphology to the independent processing parameters. However the copper coatings were too ductile to obtain good fracture specimens for cross section analysis. Figures 31-36 reveal much

Table 8 - X-ray Diffractometry of Cu Coatings on Ni Substrates

Sample	Sputter Cleaning	Plating Bias	Relative Intensity			
			(111)	(200)	(220)	(311)
Ni Substrate	--	--	100.0	30.6	26.0	13.0
			(111)	(200)	(220)	(311)
5	No	No	100.0	88.2	15.9	5.6
6	Yes	No	100.0	34.0	14.4	11.1
7	Yes	2.15	100.0	17.6	3.7	1.5
8	Yes	3.50	100.0	32.2	8.8	7.5
Cu Powder	--	--	100.0	46.0	20.0	17.0

about the effects of sputter cleaning and substrate bias durring coating deposition. Figure 31 is a SEM image of a cross-section of the evaporated copper coating without sputter cleaning. It reveals the columnar nature of the coating. Figure 32, a broadface image of the same coating, shows the columns have domed tops and reveals a crack network in the coating with a spacing similar to the grain size of the substrate. The evaporated copper coating with sputter cleaning (figure 33) has larger domes and fewer cracks. The 2.15 kV bias ion plated copper coating has better defined columns (figure 34) with a finer size and less surface roughness (figure 35) than the evaporated coatings. This coating has more cracks than the sputter cleaned evaporated copper coating but fewer cracks than the non-sputter cleaned copper coating. Figure 36 is a broadface image of the 3.5 kV bias ion plated coating. It has the smoothest surface and the fewest cracks. It appears that the column tops are refined (smaller) compared to the other coatings. Again the SEM gives infomation about the coating structure but does not supply the information desired about the coating/substrate interface. Examination of the interface is necessary to better understand the ion plating process as well as the adhesion data and is accomplished using cross-section TEM and scanning Auger depth profile analysis.

5. Transmission Electron Microscopy

Figures 37-40 comprise the TEM and EDX analysis of the

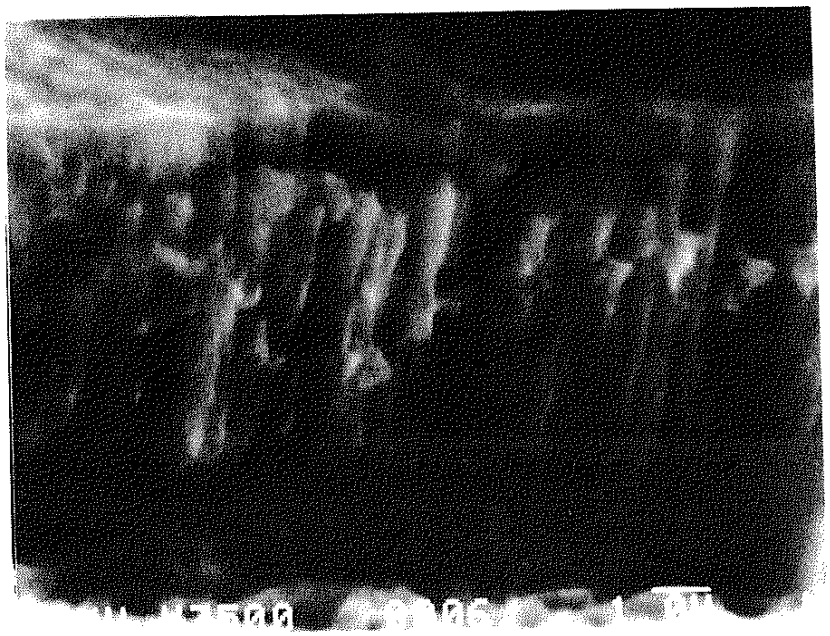

Figure 31 - Cross-section SEM of evaporated copper coating on non-sputter cleaned nickel substrate

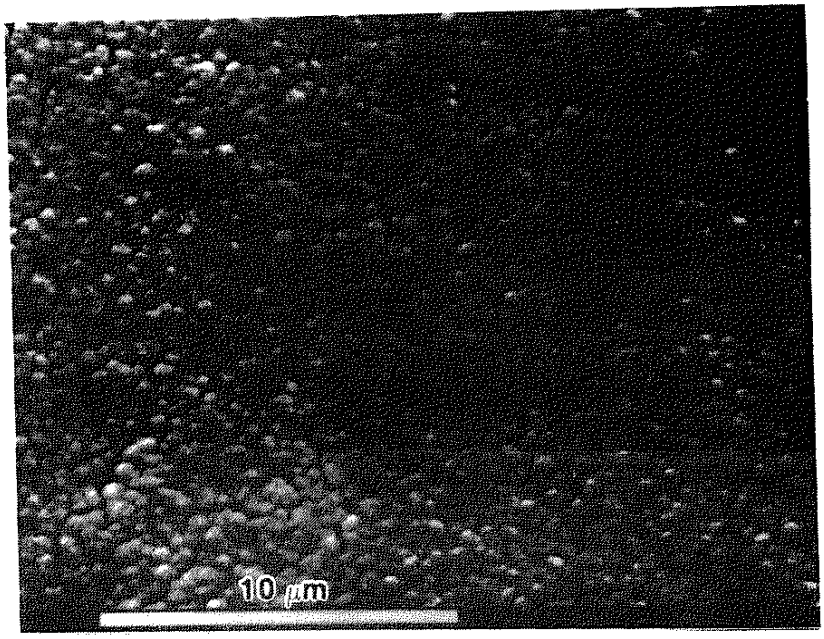

Figure 32 - Broadface SEM of evaporated copper coating on non-sputter cleaned nickel substrate

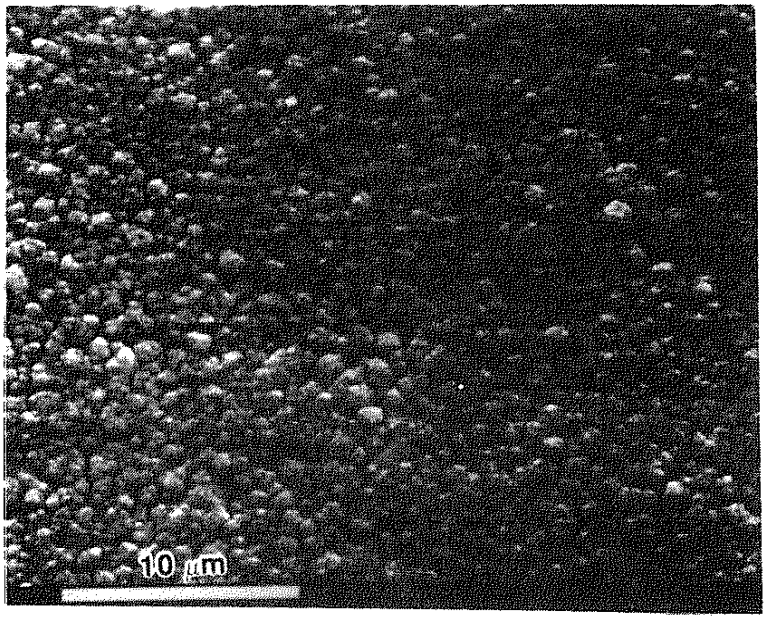

Figure 33 - Broadface SEM of evaporated copper coating on sputter cleaned nickel substrate

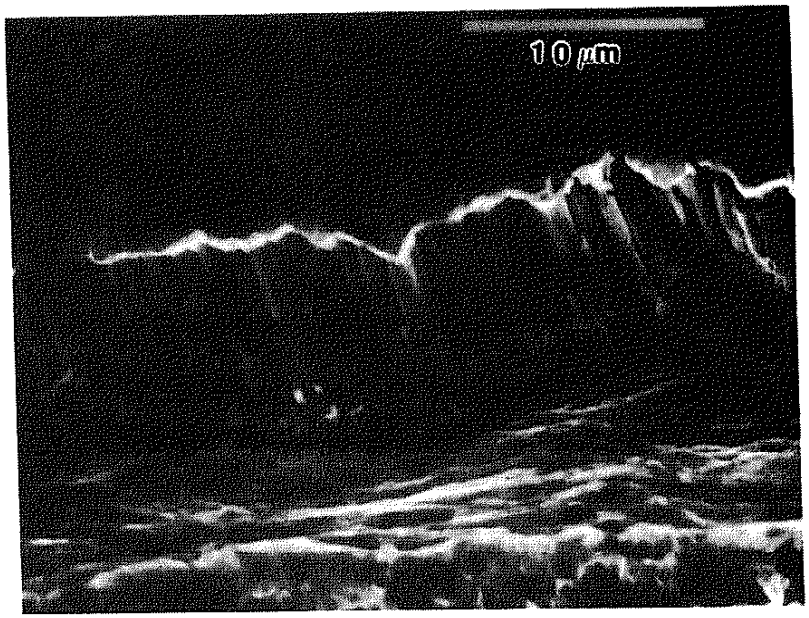

Figure 34 - Cross-section SEM of 2.15 kV bias ion plated copper coating on sputter cleaned nickel substrate

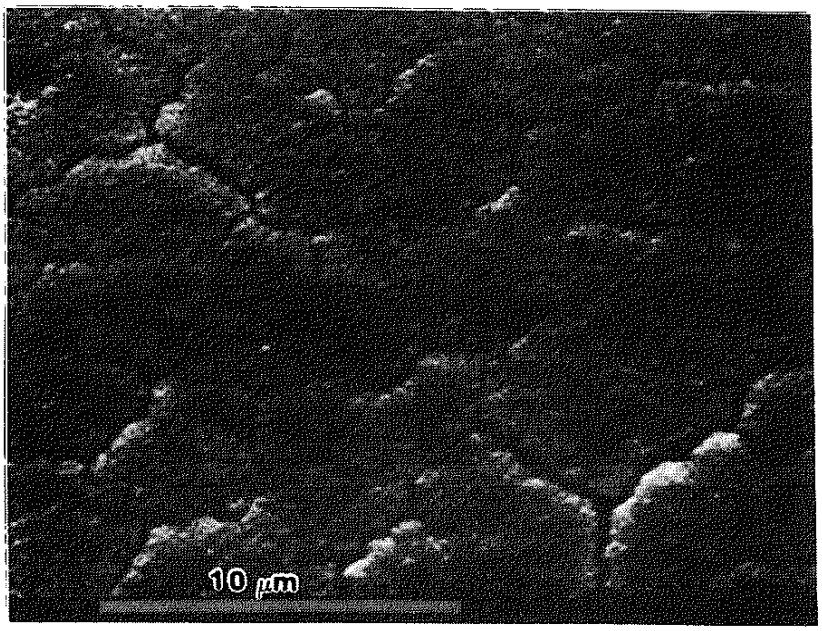

Figure 35 - Broadface SEM of 2.15 kV bias ion plated copper coating on sputter cleaned nickel substrate

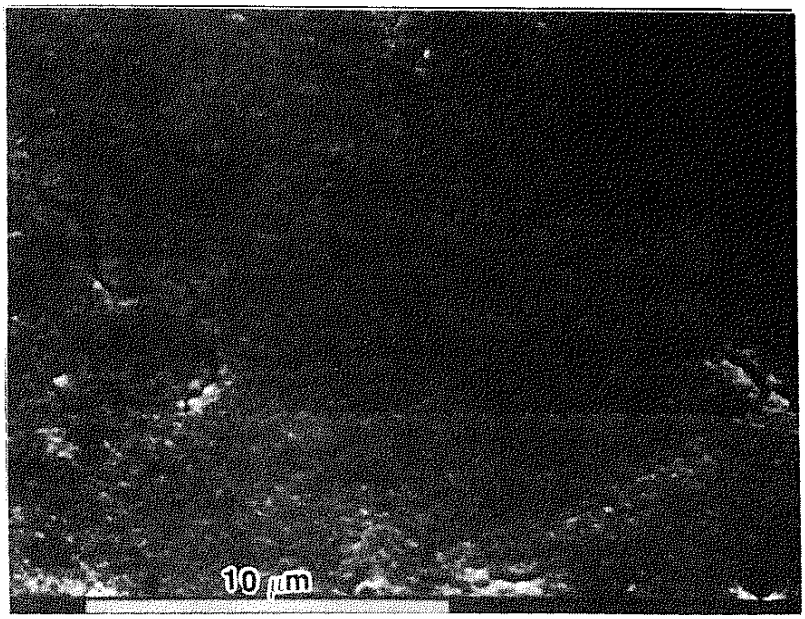

Figure 36 - Broadface SEM of 3.5 kV bias ion plated copper coating on sputter cleaned nickel substrate

evaporated copper coating on a sputter cleaned nickel substrate (coating #6). Figure 37 is a bright field image which shows a porous columnar morphology. As with the sputter cleaned chromium coatings, a 300 Å layer is present in the substrate. No such layer is evident in the coating. Figure 38, a dark field micrograph of this coating, shows the microcrystalline nature of the coating. Close examination reveals that the layer in the substrate has very little crystalline nature. EDX analysis of this coating (figures 39-40) reveals no mixing of the coating (copper) and substrate (nickel) elements. The layer in the substrate is likely a deformation layer caused by sputter cleaning. Figures 41-45 are the TEM and EDX analysis of the 2.15 kV bias ion plated copper coating on a sputter cleaned nickel substrate (#7). The bright field micrographs (figures 41 and 42) show the coating transforms from a dense rather equiaxed structure (300 Å thick nucleation layer) to a porous columnar morphology with many twins. A sputter damage layer (300 Å thick) is present in the substrate, but no visible layer exists in the coating. The EDX analysis of this sample (figures 43 and 44), however, shows a chemically mixed interface for about 500 Å into both the coating and the substrate for a total width of 1000 Å. Figure 45 is an electron diffraction pattern of the coating showing the random orientation of the crystals (see table 9 for the ring analysis).

Figures 46-47 are the TEM analysis of the 3.5 kV bias ion plated copper coating on a sputter cleaned nickel substrate (#8). The bright field micrograph (figure 46) shows two distinct layers

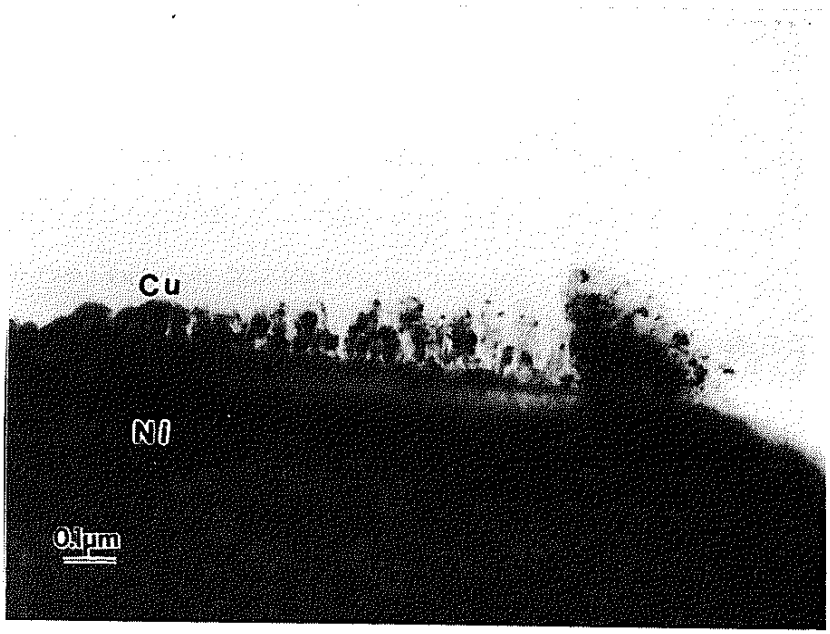

Figure 37 - TEM of evaporated copper coating on sputter cleaned nickel substrate (bright field)

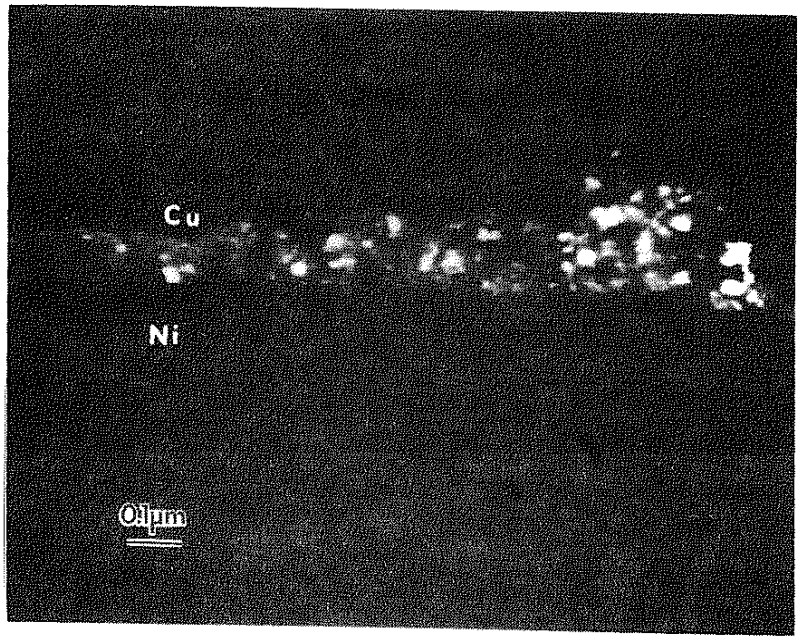

Figure 38 - Dark field image corresponding to figure 37

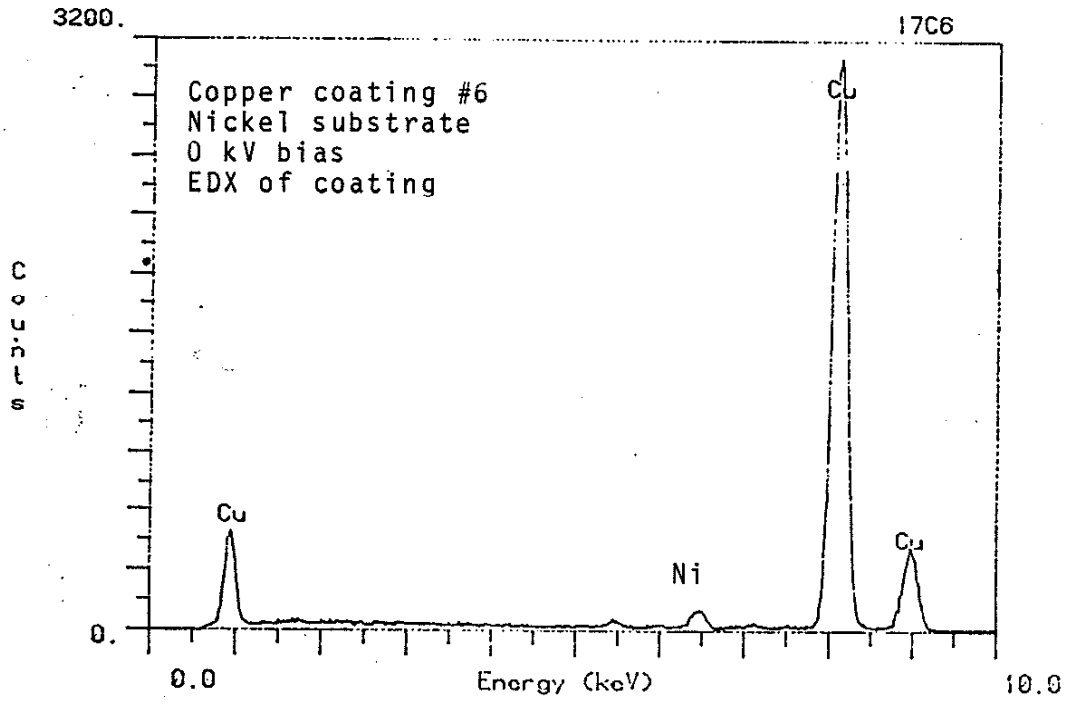

Figure 39 - EDX scan of evaporated copper coating on sputter cleaned nickel substrate, 200 Å from the interface

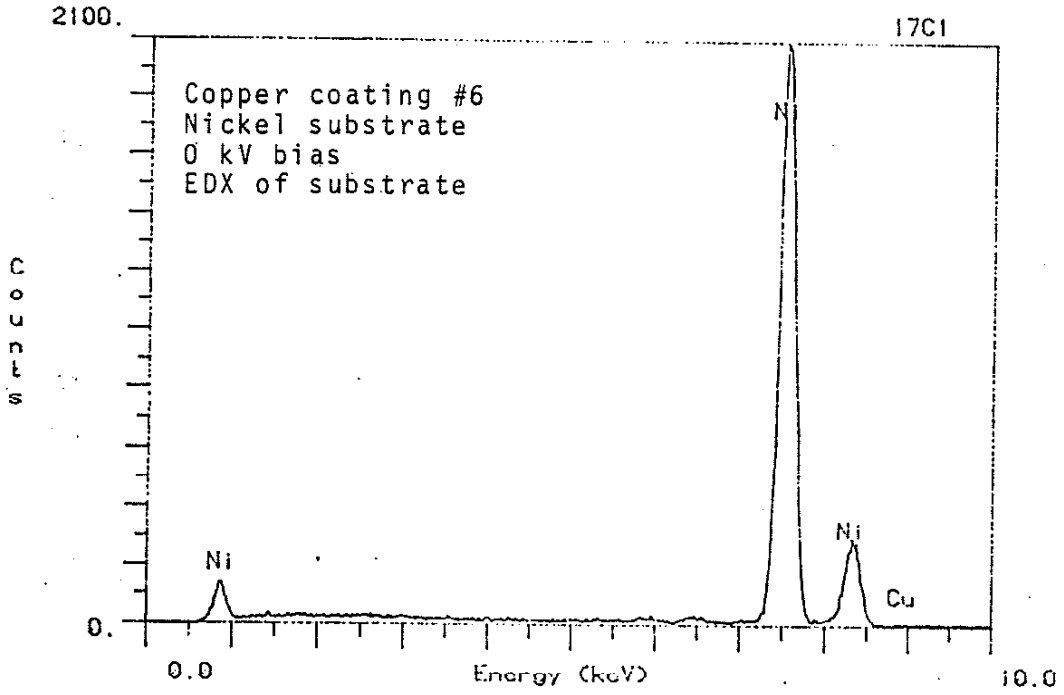

Figure 40 - EDX scan of nickel substrate of evaporated copper coating on sputter cleaned nickel substrate, 200 Å from the interface

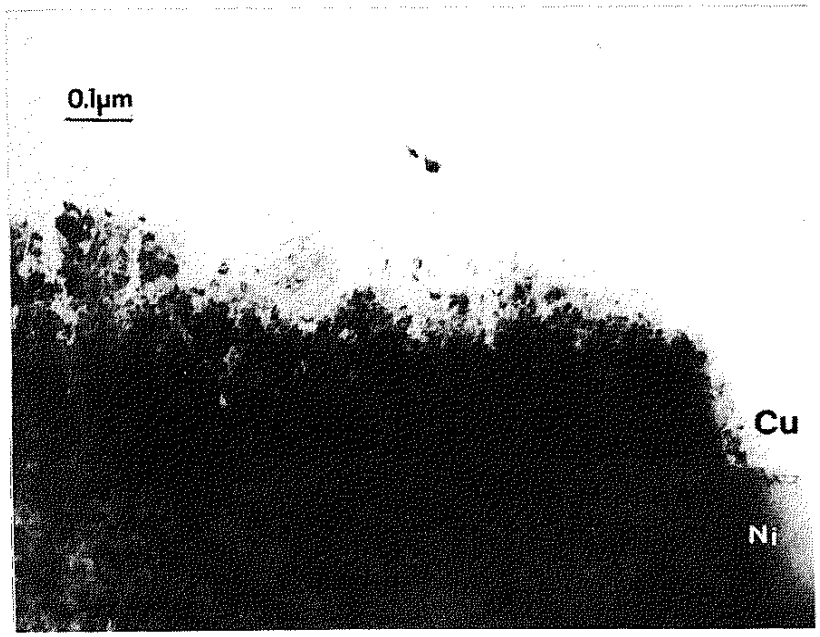

Figure 41 - TEM of 2.15 kV ion plated copper coating on sputter cleaned nickel substrate (bright field)

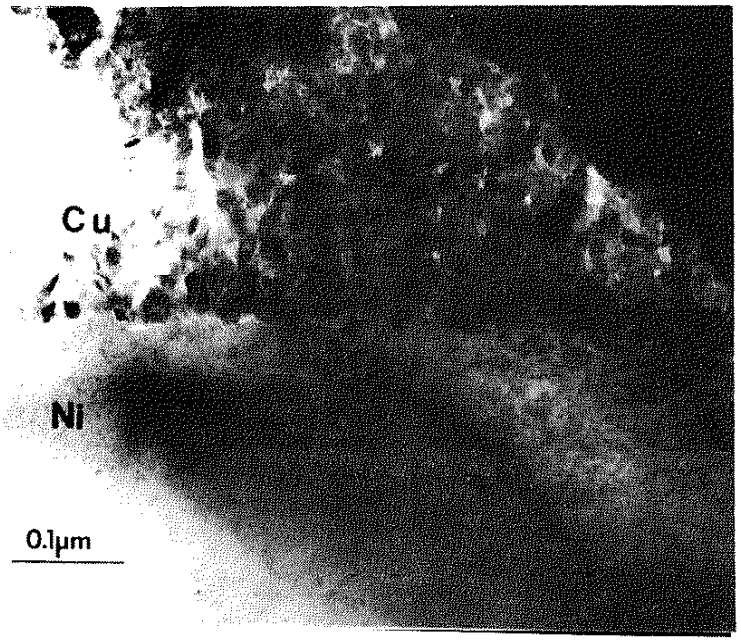

Figure 42 - TEM of 2.15 kV ion plated copper coating on sputter cleaned nickel substrate (bright field)

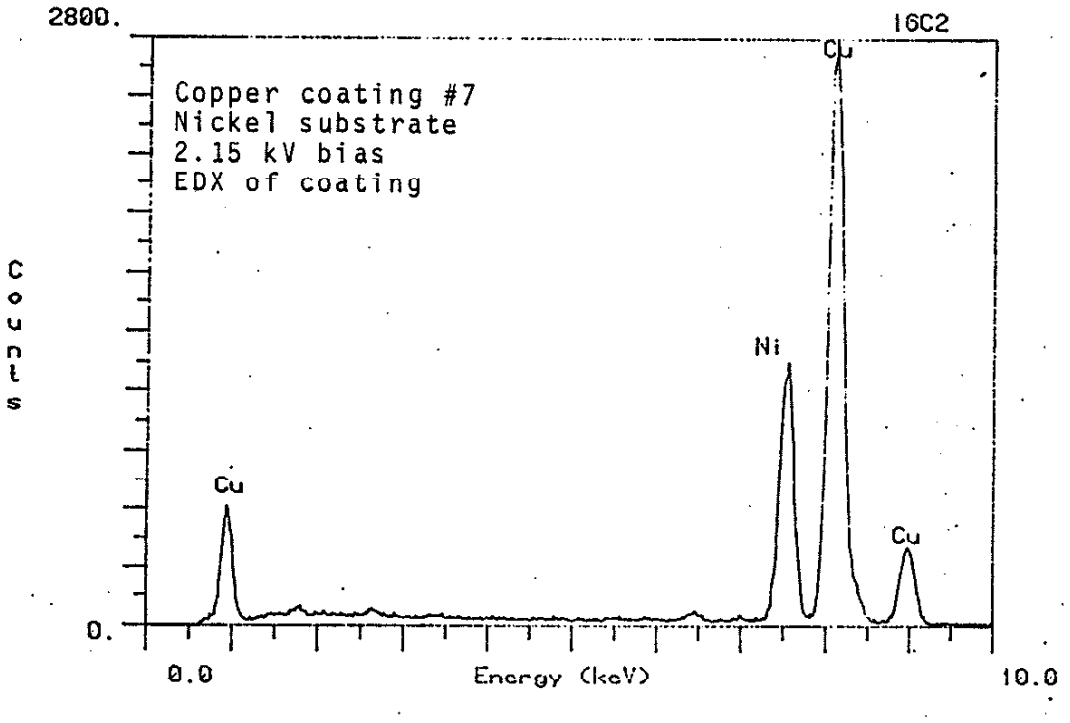

Figure 43 - EDX scan of 2.15 kV ion plated copper coating on sputter cleaned nickel substrate, 500 Å from the interface

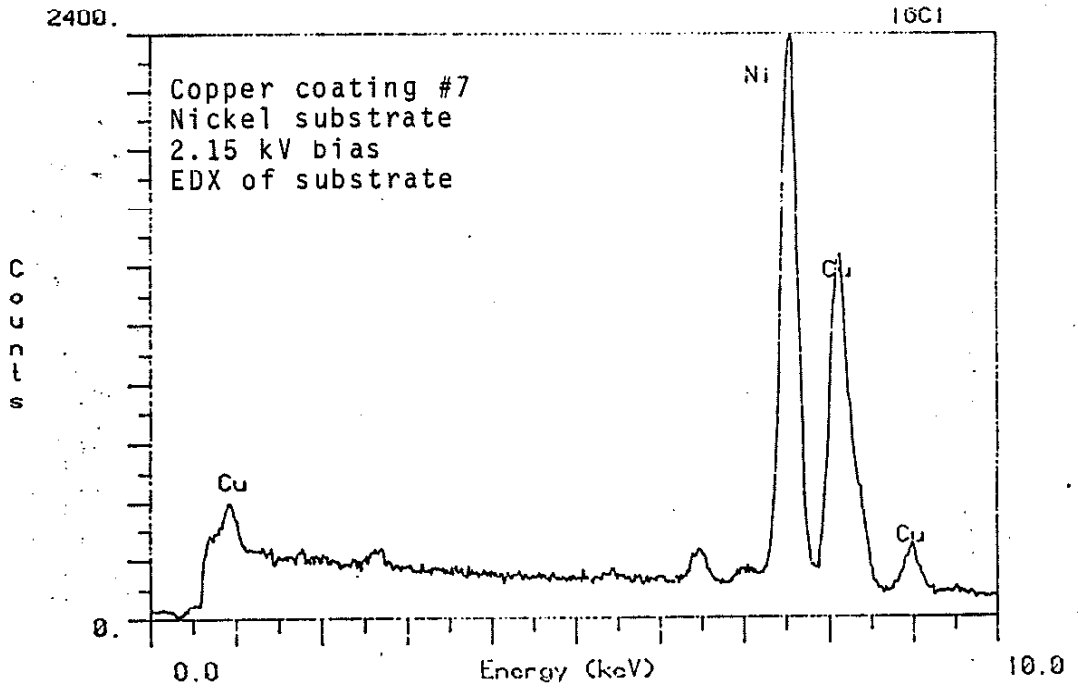

Figure 44 - EDX scan of nickel substrate of 2.15 kV ion plated copper coating on sputter cleaned nickel substrate, 500 Å from the interface

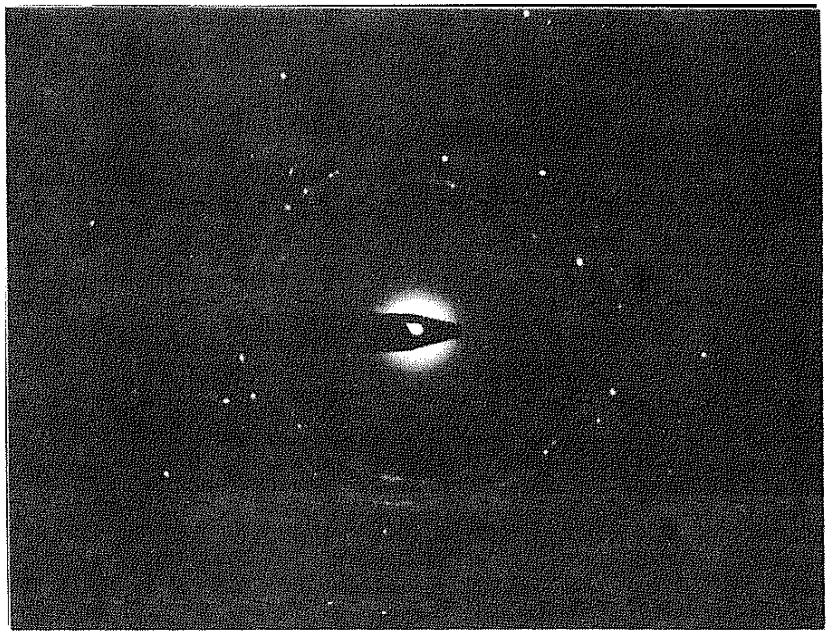

Figure 45 - Selected area electron diffraction pattern of 2.15 kV ion plated copper coating on sputter cleaned nickel substrate

Table 9 - Copper Electron Diffraction Pattern Analysis

Ring Number	Copper Crystallographic Plane
1	*
2	111
3	200
4	*
5	220
6	311
7	*

* Rings 1,4,7 correspond to the (111), (220) and (420) planes of CuO_2 respectively

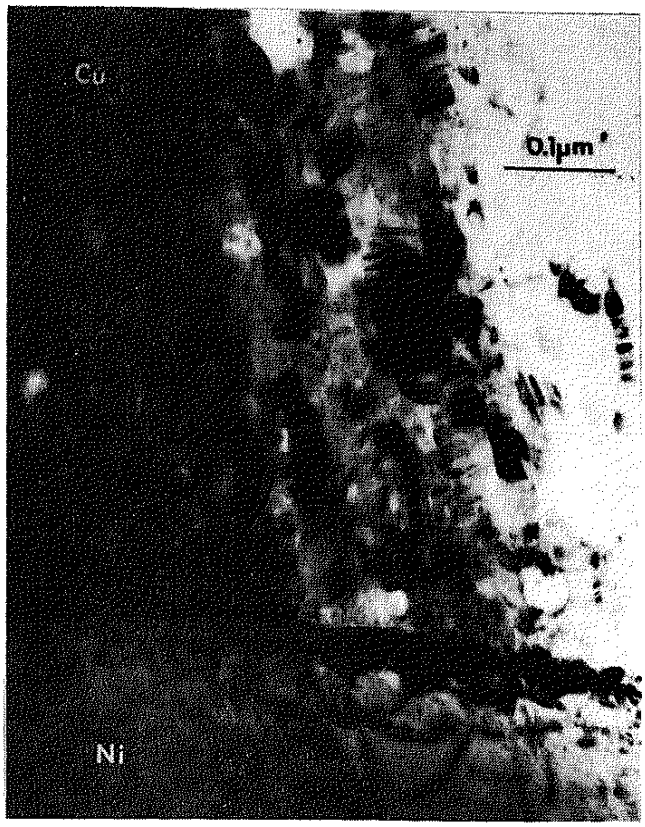

Figure 46 - TEM of 3.5 kV ion plated copper coating on sputter cleaned nickel substrate (bright field)

at the interface. One is 300 Å wide on the substrate side while the other is 150 Å wide on the coating side. The coating is very dense and has an equiaxed structure for the first 750 Å of growth before evolving into an open columnar morphology. The columns contain many heavily twinned crystals. The dark field image (figure 47) reveals the low crystalline nature of the interfacial layers. EDX analysis (not presented here) of this coating also showed an approximately 1000 Å wide chemically graded interface both into the coating and into the substrate for a total width of 0.2 μm. Electron diffraction patterns of all the copper coatings contain ring patterns demonstrating the fine grain size of the coatings.

6. Auger Analysis

Auger depth profiling was performed on two copper coatings (evaporated with sputter cleaning and 3.5 kV bias ion plated samples). No Auger analysis was performed on the adhesion pull stubs. Depth profiling was performed after the coatings had been mechanically thinned using the flattening tool on the dimpler. Thinning continued until the substrate was exposed in some areas. The depth profiles occured in the thinned regions of the coating adjacent to the exposed substrate. As with the chromium coatings, the copper was still too thick for quick analysis.

The evaporated coating with sputter cleaning requires 50 minutes for sputtering through the interface (figure 48). This

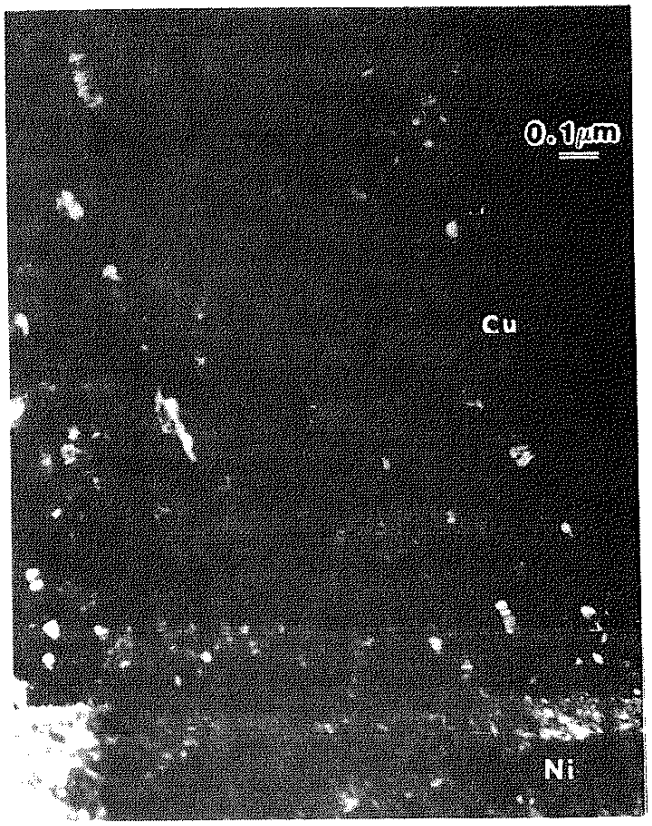

Figure 47 - Dark field image of 3.5 kV ion plated copper coating on sputter cleaned nickel substrate

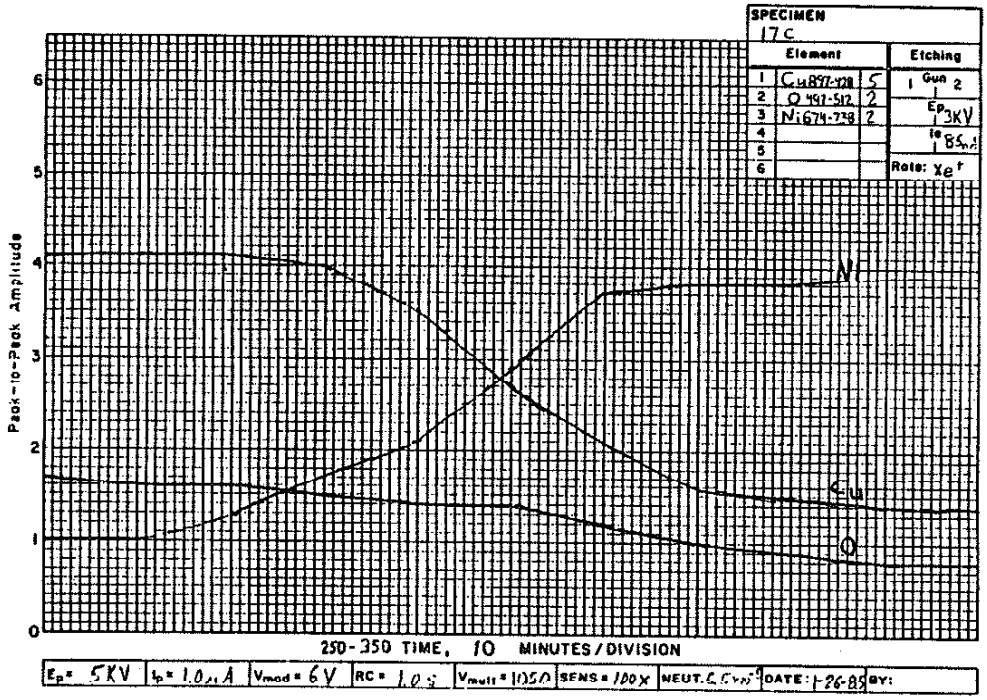

Figure 48 - Auger depth profile of evaporated copper coating on sputter cleaned nickel substrate

corresponds to approximately an 0.83 μm wide interface. This is in sharp disagreement with the TEM analysis where no chemical mixing was found.

The 3.5 kV bias ion plated copper coating (#8) requires 88 minutes for sputtering through the interface which corresponds to an interface which is 1.47 μm wide (figure 49). Figure 50 is the Auger surface survey just after depth profiling had begun. This coating contains very little oxygen contamination.

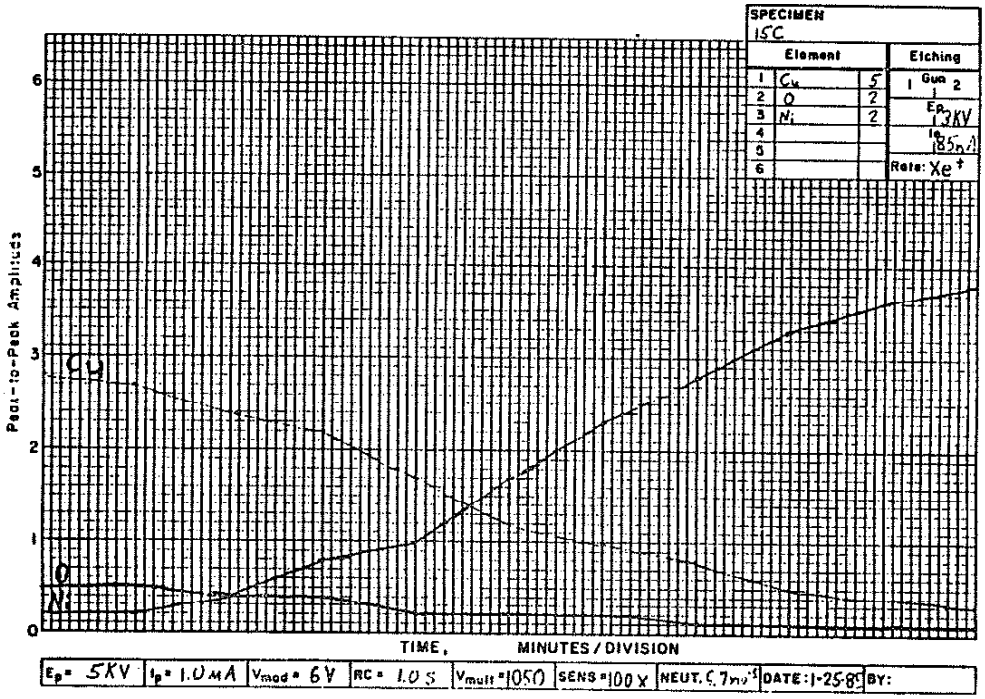

Figure 49 - Auger depth profile of 3.5 kV ion plated copper coating on sputter cleaned nickel substrate

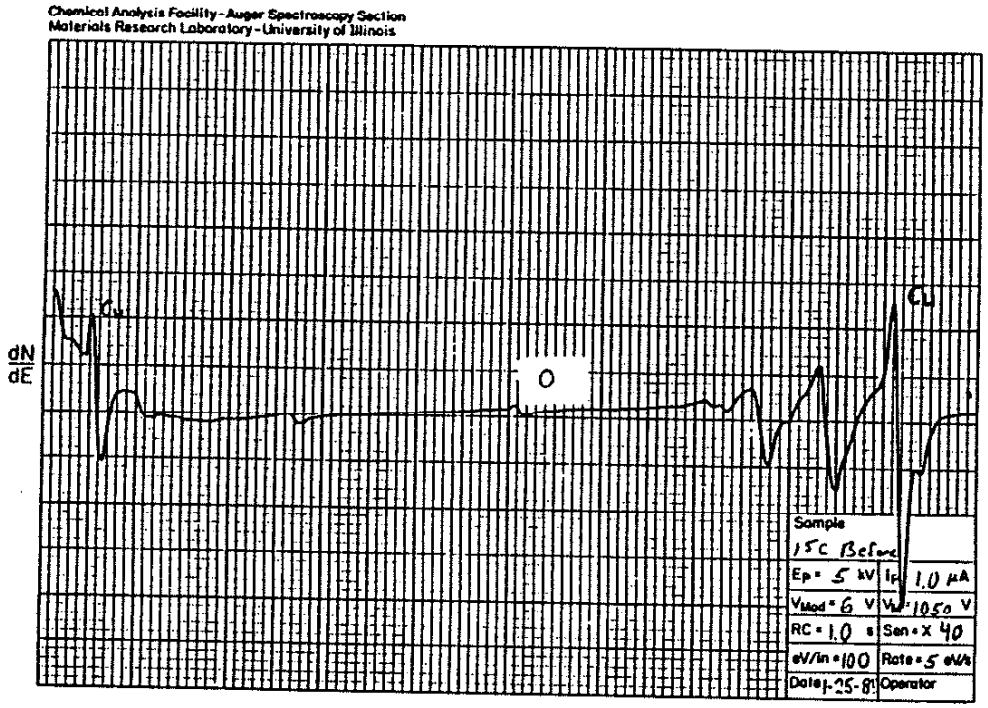

Figure 50 - Auger surface survey of 3.5 kV ion plated copper coating on sputter cleaned nickel substrate

V. Discussion

A. Sputter Cleaning

Sputter cleaning is expected to remove surface contaminants [7] providing an atomically clean surface [8], which is highly reactive [9], on which deposition occurs. Auger analysis of substrates used in the sputter cleaning rate experiment confirms that the surface is clean as no contmination due to back sputtered elements is found on the substrate. The clean surface exists because 0.10 μm of substrate material generally is removed during the sputter cleaning process used in this research. Even if back sputtering were a problem, its effects should have been eliminated by precoating the chamber with the same material as used for evaporation. Auger analysis of the coating/substrate interfaces again substantiates that no contamination due to back sputtering is present. The effects of of sputter cleaning on adhesion strength and on the microstructure of the coatings will be discussed in later sections.

B. Properties

1. Thickness

For the chromium and copper coatings a trend in the

deposition rate is evident. The evaporated coatings on the non-sputter cleaned substrates are the thickest. The evaporated coatings on the sputter cleaned substrates are the second thickest. The thickness again decreases as the ion plating bias is initiated and continues to decrease as the bias is increased. The reduction in the coating rate is similar in magnitude to the sputter rate (except for the non-sputter cleaned chromium coating which was deposited under different conditions). As all other parameters were kept constant the reduction in the coating rate is due to sputter removal. This demonstrates that the coating rate is determined by the difference between the rate at which atoms add to the surface and the rate at which atoms are sputtered away from the surface.

2. Adhesion

The use of sputter cleaning improved the adhesion of evaporated chromium coatings on copper substrates and copper coatings on nickel and copper substrates. No evidence of an extensive chemically mixed zone is found by TEM/EDX examination of the evaporated coatings. TEM revealed a sputter damaged layer in the substrates which received sputter cleaning. The increase in adhesion is explained by four processes: firstly, according to Hagstrum and D'Amico [8], sputter cleaning provides a clean surface to promote metal-metal atomic bonding between the substrate and the coating. The second reason for increased adhesion is that sputter cleaning provides a surface damaged

layer with increased surface roughness, according to Chapman [43], thus increasing the contact area between the substrate and the coating as well as promoting interlocking mechanical bonding (described by Mital [59]). This damaged layer may also aid a very localized enhanced diffusion (a few atom layers) due to a high defect concentration. Further, this damaged layer may contain conveniently located low energy sites at which coating atoms may condense [10,11] when compared to a non-damaged flat substrate. The last reason may be the most important for coatings on dissimilar materials. Evaporated copper coatings on non-sputter cleaned copper substrates have good adhesion. The increase in adhesion of this system due to sputter cleaning is small and probabally is due solely to providing a clean surface on which to deposit. A damaged layer would not be a lower energy site for the copper on copper case (as there is no lattice mismatch) nor is mechanical bonding important compared to metallic bonding.

The evaporated chromium coatings on copper substrates and evaporated copper coatings on nickel substrates have dramatic increases in adhesion due to sputter cleaning. If the contributions to the increased adhesion due to a clean surface and due to a rough surface are again small, then the low energy sites, present in the damaged layer, where the coating atoms condense may be the most important cause of the increased adhesion.

The use of an ion plating bias also increases the adhesion of the copper coatings (in agreement with Stoddart et al. [66] and

Swaroop and Adler [61]). Increasing the bias also increases the adhesion. TEM and EDX analyses show a chemically mixed zone is present in these coatings. Mattox [3] shows that this delocalizes the stress of the coating due to lattice mismatch thus promoting adhesion.

The use of an ion plating bias initially increases the adhesion of chromium coatings on copper substrates, but increasing the bias from 2.15 kV to 4.0 kV causes a reduction in the adhesion strength.

The use of the Sebastian adhesion test did allow for semi-quantitative comparison of adhesion strength, but fails to give the precision and accuracy necessary for purely quantitative results. The problems with this method include data scatter and also the locus of failure may change which Good [55] says requires the use of microchemical analysis to detect.

C. Structure and Chemistry

1. X-ray Diffraction

Evaporated chromium coatings have a nearly random (110) orientation which are the most densely packed (but not close packed) in the bcc system but are not much more densely packed than several other planes. The use of a plating bias changes the preferred orientation to the (200) planes. The four (110) planes are 45° from the (200) planes for bcc materials and are likely the faces of the tops of the columns. The copper coatings all

exhibit a (111) orientation and grow on nickel substrates which also have a (111) orientation. The use of sputter cleaning and an ion plating bias enhance the (111) preferred orientation. This is as expected as the densest planes should sputter the slowest and therefore grow the fastest.

2. Scanning Electron Microscopy

The morphology of the chromium coatings revealed by SEM is consistent with that of the Thornton zone diagram [46] in most regards. The evaporated coating without sputter cleaning has a zone 1 morphology as expected since the parameters are identical to that of thermal evaporation with a working gas used by Thornton to develop his diagram. The use of sputter cleaning causes the morphology to change to a zone T type structure as the columns are less well-defined. Sputter cleaning provides many defects at which nucleation may occur, thus refining the column size. The effect of sputter cleaning is not accounted for by Thornton as all he varies is working gas pressure and substrate temperature. The use of a plating bias also is not accounted for in the Thornton diagram. In this experiment a 2.15 kV ion plating bias causes a zone 2 morphology (well defined, closely packed columns with faceted tops). Thus an increase in plating bias has a similar effect as increasing the substrate temperature. Later work by Thornton [47] included biased sputtering. He reports the use of bias suppresses columnar morphology by redistributing coating material through sputtering.

However, increasing the ion plating bias to 4.0 kV causes the columns to become loosely packed, faceted and extremely well defined. It appears that at these conditions (high bias and low pressure) the sputtering is preferential and does not redistribute material to fill in the valleys between the columns and thus favors column formation.

The use of SEM on the copper coatings was limited because good fracture cross sections could not be obtained due to copper's ductility. The evaporated coating with sputter cleaning is a zone 1 coating and has the roughest surface of the copper coatings. The copper coatings all appear a little thicker at the cracks which have about the same spacing as the nickel substrate grain size. The nickel grain boundaries may be sites of easy nucleation. Sputter cleaning reduces the number of cracks. This may be due to increasing the number of other nucleation sites. Use of a 2.15 kV ion plating bias produces a coating with a finer column size and less surface roughness than for the evaporated coatings. For the copper coatings an increase in ion plating bias causes a smoother surface in agreement with Thornton's idea of coating material redistribution [47]. The inconsistency of this coating redistribution of coating material shows the difficulty of developing universal processing parameter-structural relationships.

3. Transmission Electron Microscopy and EDX

SEM does not have the resolution necessary to study the

structure of the interfacial region. Therefore, TEM, in spite of its difficult sample preparation, is the primary tool used to study the interface. Most studies in the ion plating literature used SEM to examine the coatings, but no cross-section TEM investigations were available for comparison with this research. Cross-section TEM confirmed the presence of the morphologies determined by SEM but also revealed the presence of layers in both the substrate and the coating. Chemical analysis of these near interface layers was also perfomed in the TEM. For all of the chromium coatings on sputter cleaned copper substrates a layer about 300 Å wide is present in the substrate at the interface. EDX analysis (probe size 400 Å) of this layer shows it to be pure copper for the evaporated coating and to be a mixture of chromium and copper for the ion plated coatings. Since it is present in the evaporated sample it is thought to be caused by the sputter cleaning process. This also explains its nearly constant thickness as all the copper substrates were subjected to identical sputter cleaning parameters.

A nucleation layer 800 Å wide is found in the evaporated coating and a 400 Å wide layer is found in the 4.0 kV ion plated coating. This layer is dense and equiaxed. After this layer the coating becomes columnar. Enomto and Matsubara [33] also report a nucleation layer but on a much larger scale. They also report that the layer is thickest for the evaporated coatings. EDX analysis of this layer shows that it is pure chromium for the evaporated coating but again is a mixture of copper and chromium for the ion plated coatings. No conclusive explaination has been

developed for this growth phenomenon.

The 4.0 kV ion plated chromium coating has a main spine and secondary growth arms typical of dendritic growth of liquid to solid phase transformations. No evidence of dendritic growth in physical vapor deposition was encountered in the literature search as few researchers have used cross-section TEM to analyze their coatings. Each column of the coating is polycrystalline in disagreement with the Thornton diagram [46].

TEM of the copper coatings reveals similar trends. A deformed substrate layer (250 Å - 300 Å wide) is found in sputter cleaned nickel substrates. No extensive (less than 100 Å) chemical mixing occurs for the evaporated coatings. A chemically mixed layer is present in both the substrate and the coating for the ion plated coatings and increases with increasing plating bias. Lastly, an equiaxed nucleation layer is present in the ion plated coatings before they become columnar. This time the width of the layer increases with increasing bias in disagreement with Enomoto and Matsubara [33]. Again it is evident that these "trends" are not consistent for all materials.

4. Auger Analysis

Auger microchemical analysis was the first chemical analysis performed because the samples were much easier to produce than cross-section TEM samples. Many problems, however, were encountered in the Auger analysis. The problems include: the substrates were not flat enough thus causing cone formation and

thereby broadening the recorded interface width and the coatings were still too thick even after mechanical thinning which again caused the interfaces to appear broader than they actually are because of uneven sputtering. Thus, the Auger results are not likely accurate in a quantitative sense but are probabally good enough for a qualitative comparison.

Auger analysis was useful for several reasons. Firstly, it was used to identify the locus of failure for the chromium adhesion tests. This was especially important as the failure locus changed from the chromium/copper interface for the non-sputter cleaned evaporated coating and 4.0 kV ion plated coating to failing within the chromium coating for the sputter cleaned evaporated coating and the 2.15 kV ion plated coating. Secondly, it allows for detection of oxygen in the coatings which was not possible with the EDX system used (a great amount of oxygen is found in the chromium coatings but almost none is found in the copper coatings). Lastly, Auger depth profiles demonstrated the likelyhood of a chemically graded interface which pointed to the absolute necessity of performing cross-section TEM analysis.

The Auger results show a trend of an increased chemically graded interface width with increasing substrate bias in agreement with the TEM/EDX data. Auger analysis is thus useful as a quick way of discovering trends in interface width, but overestimates the width every time (by about a factor of 10 for cases which show a graded interface in the TEM). Thus TEM/EDX analysis should always be performed when quantitative results are desired for chemically graded interfaces.

VI. Conclusions

The adhesion of both chromium films on copper substrates and copper films on nickel substrates is improved by sputter cleaning. Sputter cleaning provides a clean and reactive surface to coat. The use of a 2.15 kV ion plating bias increases the adhesion of both systems. An increase in the ion plating bias to 3.5 kV increases the adhesion of the copper coatings, but increasing the bias to 4.0 kV causes a reduction in the adhesion of the chromium coatings, probabally due to microstructural changes in the chromium film.

Sputter cleaning also creates a damaged layer in the substrate at the substrate/coating interface. This layer has the same chemistry as the substrate. The use of an applied ion plating bias, however, causes interfacial mixing of the coating and substrate materials, characteristic of the ion plating process, as detected by both an Auger microprobe and TEM/EDX analysis.

Applied ion plating bias also changes the morphology of the coatings. Film morphology changes from dome topped, densely packed and indistinct columns (zone 1) for the evaporated coatings to faceted topped, loosely packed and distinct columnar coatings (zone 2). Equiaxed grain coatings (zone 3) were not produced and may require higher pressures and higher ion plating biases than used in this study. The column spacing also increases as the bias increases.

Ion plating bias also affcts the width of a fine grained, equiaxed nucleation layer. For the chromium coatings an increasing bias reduces the width of the nucleation layer. However, increasing the bias increases the width of this layer in copper coatings.

The use of cross-section TEM, in spite of its difficult sample preparation, is necessary to examine the structure and chemistry of the interface and the nearby damaged layer in the substrate and the nucleation layer in the coating.

Proper selection of ion plating processing parameters allows the production of adherent chromium and copper films for several film morphologies.

VII. References

1. J.M. Rigsbee, Unpublished
2. R.F. Bunshah, J. Vac. Sci. Technol. B. 2, 789, 1984
3. J.M. Walls, Thin Solid Films 80, 213, 1981
4. D.G. Teer, B.L. Delcea and A.J. Kirkham, J. Adhesion 8, 171, 1976
5. R.F. Hoch and D.M. Mattox, Metals Handbook Vol 5 9th ed., American Society for Metals, Metals Park, 420, 1985
6. R. Bahl, H.K. Pulker and E. Moll, Thin Solid Films 80,221, 1981
7. G. Wehner, Science and Technol 81, 32, 1968
8. H.D. Hagstrum and C. D'Amico, J. Applied Physics 31, 715 1960
9. D.M. Mattox, J. Vac. Sci. Technol. 10, 47, 1973
10. K.L. Chopru J. Applied Physics 37, 2249, 1969
11. P.E. Bovey, Vacuum 19, 497, 1967
12. J.M. Walls, Thin Solid Films 80, 213, 1981
13. D.G. Teer, J Adhesion 8, 289, 1977
14. D.G. Teer, B.L. Delcea and A.J. Kirkham, J. Adhesion 8, 1976
15. K.H. Kloos, E. Broszeit and H.M. Gabriel, Thin Solid Films 80, 1981
16. G. Carter, J. Vac. Sci. Technol. 7, 488, 1970
17. L.I. Maissel and R. Glang, Handbook of Thin Film Technology Mc Graw Hill, New York, 4, 1970
18. D.M. Mattox, Sandia Corp., Monograph SC-R-65-852, 1965

19. D.G. Teer and B.L. Delcea, Thin Solid Films 54, 295, 1978

20. M. Lardon et al., Thin Solid Films 54, 317, 1978

21. B.A. Movchan and A.V. Demchishin, Fiz. Metall. Metalloved 28, 653, 1969

22. D.M. Mattox and G.J. Kominiak, J. Vac Sci Technol 9, 528, 1972

23. K.L. Chopru, J. Applied Physics 37, 2249, 1969

24. P.E. Bovey, Vacuum 19, 497, 1967

25. D.M. Mattox, Trans SAE, 2175, 1969

26. D.M. Mattox and R.D. Bland, J. Nuc. Materials 21, 349, 1967

27. D.M. Mattox, Electrochemical Technology 2, 245, 1964

28. K.E. Stenke and L.E. Mc Crary J. Vac. Sci. Technol. 13, 82, 1976

29. D.G. Teer and F. Salem, Thin Solid Films 45, 583, 1977

30. B. Bergbars, British Patent 510 933, 1968

31. K.H. Kloos, E. Broszeit and H.M. Gabriel, Thin Solid Films 80, 307, 1981

32. N. Ohami, J. Vac. Sci. Technol. 13, 82, 1976

33. Y. Enomoto and K. Matsubara, J. Vac. Sci. Technol. 12, 827, 1975

34. R. Bahl, H.K. Pulker and E. Moll, Thin Solid Films 80, 221, 1981

35. N.J. Archer, Thin Solid Films 80, 221, 1981

36. T. Sato et al., Thin Solid Films 54, 61, 1978

37. B. Zega, M. Kornmunn and J. Amignet, Thin Solid Films 45, 517, 1977

38. B. Chapman, Glow Discharge Processes, John Wiley and Sons, New York, 1980

39. W.D. Davis and T.A. Vanderslice, Physical Reviev 131, 219, 1963

40. W.D. Davis, Ibid

41. J.E. Houston and J.E. Uhl, Sandia Corp. Monograph SC-RR-71-0211, 1971

42. D.G. Armour et al., Vacuum 34, 295, 1984

43. B. Chapman, Glow Discharge Processes, John Wiley and Sons, New York, 1980

44. D.M. Mattox, Proc. Conf. Ion Plating and Allied Techniques, C.E.P. Consultants, Edinburgh, 1977

45. B.A. Movchan and A.V. Demchishin, Fiz. Metall. Metalloved 28, 653, 1969

46. J.A. Thornton, J. Vac. Sci. Technol. 12, 830, 1975

47. J.A. Thornton, Thin Solid Films 40, 335, 1977

48. H. Oechsner, J. of Physics 8, 198, 1975

49. P. Sigmund, Physical Review 184, 383, 1969

50. J.E. Greene, CRC Critical Review in Solid State and Material Sci 11, 47, 1983

51. J. Bohdansky et al., J. of Physics 52, 2861, 1980

52. A.H. Eltoukhy and J.E. Greene, J. of Physics 51, 4444, 1980

53. D.R. Gaskell, Introduction to Metallurgical Thermodynamics, Mc Graw Hill, New York, 167, 1981

54. L.I. Maissel and R. Glang, Handbook of Thin Film Technology Mc Graw Hill, New York, 4, 1970

55. K.L. Mital, ed., Adhesion Measurement of Thin Films, Thick Films and Bulk Coatings, American Society for Testing and Materials, Philadelphia, 5, 1978

56. K.L. Mital, ed., Ibid, 18

57. K.L. Mital, ed., Ibid, 54

58. D.M. Mattox, Thin Solid Films 18, 173, 1973

59. K.L. Mital, ed., Adhesion Measurement of Thin Films, Thick Films and Bulk Coatings, American Society for Testing and Materials, Philadelphia, 54, 1978

60. R. Jacobson and B. Kruse, Thin Solid Films 15, 71, 1973

61. D.M. Mattox, Sandia Corp., Monograph SC-R-65-852, 1965

62. K.L. Mital, ed., Adhesion Measurement of Thin Films, Thick Films and Bulk Coatings, American Society for Testing and Materials, Philadelphia, 355, 1978

63. S.A. Varchenya and G.P. Upit, Thin Solid Films 122, 59, 1984

64. J. Salem and F. Sequida, J. Vac. Sci. Technol. 18, 149, 1981

65. M.J. Mirtich, J. Vac. Sci. Technol. 18, 186, 1981

66. C.T.H. Stoddart et al., J. Adhesion 2, 270, 1970

67. A. Kikuchi, S. Baba and A. Kinbura, Thin Solid Films 124, 343, 1985

68. A.J. Perry and H.K. Pulker, Thin Solid Films 124, 323, 1985

69. A. Aberman and H. Martinez, Thin Solid Films 115, 185, 1984

70. J. Walls et al., Thin Solid Films 54, 303, 1978